Metal-Organic-Framework-Based Cathodes for Enhancing the Electrochemical Performances of Batteries

A Review

Wang, Z.Y.; Tao, H.Z.; Yue, Yuanzheng

Published in:
ChemElectroChem

DOI (link to publication from Publisher):
10.1002/celc.201900843

Publication date:
2019

Document Version
Accepted author manuscript, peer reviewed version

FUNDAMENTALS & APPLICATIONS

CHEMELECTROCHEM

ANALYSIS & CATALYSIS, BIO & NANO, ENERGY & MORE

Accepted Article

Title: Metal-organic frameworks based cathodes for enhancing electrochemical performances of batteries: a review Zhaoyang Wang,[a] Haizheng Tao*[a] and Yuanzheng Yue*[a, b, c]

Authors: Zhaoyang Wang, Haizheng Tao, and Yuanzheng Yue

To be cited as: *ChemElectroChem* 10.1002/celc.201900843

Link to VoR: http://dx.doi.org/10.1002/celc.201900843

A Journal of

ChemPubSoc Europe

WILEY-VCH

www.chemelectrochem.org

Metal-organic frameworks based cathodes for enhancing electrochemical performances of batteries: a review

Zhaoyang Wang,[a] Haizheng Tao*[a] and Yuanzheng Yue*[a, b, c]

Abstract: Owing to their huge specific surface areas, high porosity, abundant metal active-sites, adjustable structure and tunable pore diameters, metal-organic frameworks (MOFs) have attracted much attention of the battery scientists and technologists. MOFs have proven to be versatile precursors of cathode materials for batteries, and the MOF-based cathodes have already exhibited excellent electrochemical performances. In this article, we review some recent advances in developing MOFs-derived cathodes for lithium/sodium ion batteries, lithium-sulfur batteries, lithium-air batteries, and lithium-selenium batteries. We also describe the synthetic mechanism, characterization of MOFs-derived cathodes, and the origin of the enhanced electrochemical performances. Finally, we point out some challenges and opportunities for the future development of MOFs-based cathodes.

1. Introduction

Hybrid electric vehicles (HEVs) and electric vehicles (EVs) have become one of the most promising solutions for solving the energy and environmental issues of our planet.[1-3] During this process, secondary batteries have attracted much attention due to its high energy density, small volume and environment benefits. Lithium ion batteries (LIBs) have been commercialized and widely used in portable electronic devices[4,5] and in other occasions.[6,7] Although LIBs are still dominant in many applications, sodium ion batteries (SIBs) are emerging due to their availability in nature source and lower compared to LIBs. SIBs have been regarded as an alternative promising solution for electrical power system.[8-10] Lithium-sulfur (Li-S) batteries,[11] lithium-air (Li-O_2) batteries[12] and lithium-selenium (Li-Se) batteries[13] have been widely exploited to enhance the electrochemical performances of energy storage systems.

LIBs are widely used in various electrical and electronic devices owing to their high capacities and high energy densities.[14] However, lithium resources cannot satisfy the increasing market demands. Given the abundant reserves of sodium, as well as its similar physical and chemical properties to those of lithium,[15] SIBs are considered to be a cost effective choice for large scale energy storage and conversion. However, LIBs, and especially SIBs, has the poor high-rate performances. Many efforts (such as downsizing the particles of electrode materials,[16] conductive materials coating,[17] elemental doping[18] and structural design[19]) have been made to improve the high-rate performances of both kinds of batteries. Recently, Li-S/Se batteries appear to be a promising one for high power required devices owing to their higher theoretical specific capacity compared to LIBs and SIBs.[20,21] It should be mentioned that there is a huge challenge for functional applications of Li-S/Se batteries, e.g., the shuttle effect of the intermediates (Li_2S/Se_n, n>2) in organic liquid electrolyte.[22] Confining S/Se into the porous hosts is a widely applied strategy to restrain shuttle effect, due to the immobilization of the generated intermediates by physical and/or chemical adsorptions.[23] Li-O_2 batteries possess higher theoretical gravimetric energy density than other chemical batteries.[24] It is well known that the Coulombic efficiency of Li-O_2 battery is poor. Design of cathode materials with special structure and catalytic activity is an effective approach to improve the Coulombic efficiency of Li-O_2 batteries.[25,26] Above all, the ideal cathode materials for the above-mentioned batteries should have the characteristics of unique morphology, porosity and even catalytic activity.

Metal-organic frameworks (MOFs) were first discovered and defined by Yaghi and co-workers in 1995.[27] As a kind of new porous electrode materials, MOFs have become a new research hotspot in energy storage materials due to their huge specific surface area, unique morphology, multifunctional organic linkers and controllable pore structures. MOFs are composed of metal sites (such as transition metals, alkaline earth metals or lanthanides) and organic linkers (imidazole, pyridyl, carboxylates, polyamines and so on).[28] A growing number of MOFs have been investigated.[29-31] More importantly, MOFs have been used as versatile precursors or templates for synthesizing electrode materials.[9,32-34] There are three major advantages of using MOFs as precursors or templates for preparing electrode materials of batteries. First, it is easy to regulate the morphology and structure of MOFs for controlling ionic and electronic transfer kinetics. Second, MOFs can offer nanoporous structure with a controllable pore size and geometry to promote the infiltration of electrolyte and increase cyclic stability of charge/discharge progress. Finally, the organic ligands can be modified with doped nitrogen to improve the electrical conductivity and electrochemical activity of the resulting nanomaterials.[35,36]

MOFs are constructed by the coordination bonds between metal nodes and organic linkers. Such weak bonds not only result in poor structure stability of MOFs, but also lead to low yield of MOFs. Synthetic process is critical for

[a] Z. Wang, Prof. H. Tao, Prof. Y. Yue
State Key Laboratory of Silicate Materials for Architectures
Wuhan University of Technology
Wuhan 430070, China
E-mail: yy@bio.auu.dk (Y.Z. Yue)
thz@whut.edu.cn (H.Z. Tao)
[b] Prof. Y. Yue
Department of Chemistry and Bioscience
Aalborg University
DK-9220 Aalborg, Denmark
[c] Prof. Y. Yue
School of Materials Science and Engineering
Qilu University of Technology
Jinan 250300, China

acquiring high quality MOFs crystals. In view of the natural defects of MOFs, several synthesis methods such as room-temperature synthesis,[37,38] hydrothermal,[39-41] solvothermal,[42,43] sonochemical synthesis[44] and microwave synthesis[45,46] have been applied to enhance the quality of MOFs. In spite of the advantages of these synthetic methods, they all inevitably generate precipitates in the synthesis process, which make it difficult to introduce MOFs into cathode. Therefore it is crucial to develop an effective method for synthesizing suitable MOFs that is capable of enhancing the electrochemical performances of cathode materials.

In the past few years, several review articles have addressed the progress in developing MOFs to be used in energy storage and conversion systems.[28,29,47-50] However, it is hard to find review articles that deal with only the MOF-based cathodes for batteries. Therefore, in this article, we give a detailed review on the advances in development of MOF-modified cathode materials for batteries during the past two decades, especially during the last five years. It is known that the capacity of traditional cathode materials is much lower than anode materials.[51,52] Capacity mismatch gives rise to not only the wasted capacity of anode materials, but also the limitation of battery development. Since cathode materials often possess a complex composition, it is difficult to introduce MOFs into cathode materials without sacrificing the MOFs' advantages. This article focuses on some of the new results in developing MOF-modified cathodes for LIBs, Li-S batteries, Li-O_2 batteries and Li-Se batteries. Finally, we discuss the challenges and perspectives for the future research of MOF-modified cathodes for batteries.

Zhaoyang Wang received his B.S. and M.S. degrees from Qilu university of Technology in 2014 and 2017, respectively. He is currently a PhD student under the supervision of Professor Yuanzheng Yue in State Key Laboratory of Silicate Materials for Architectures from Wuhan University of Technology. His research interests mainly focus on full glass-ceramic Li/Na ion batteries.

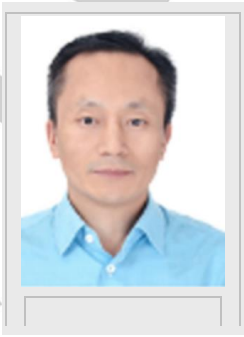

Haizheng Tao is Chair Professor of State Key Laboratory of Silicate Materials for Architectures at Wuhan University of Technology (WUT). He received his Ph.D. from WUT in 2004. He is the author of over 150 scientific papers and 31 granted patent. He is the vice chair of Special Glass Branch of the Chinese Ceramic Society. His current research interests focus on optical materials, energy storage materials, glasses and amorphous materials.

Yuanzheng Yue is Professor of Chemistry at Aalborg University (AAU), Denmark, and a distinguished visiting professor at Wuhan University of Technology, China. He received his Ph.D. degree from Technische Universität Berlin, Germany, in 1995. He is a council member of the International Commission on Glass (ICG), the founding chair of the ICG Technical Committee for Glass Fibers, and a member of the European Academy of Sciences. His research deals with glasses, glass fibres, insulation materials, and amorphous materials for energy storage devices.

2. MOFs-derived cathode materials for Li/Na-ion batteries

Most of cathode materials in Li/Na-ion batteries suffer from poor electroactivity. It is hard to settle this problem by relying solely on the modification of traditional cathode materials. Therefore, scientists and engineers attempt to develop new types or even new generation of cathode materials and to carry out innovative design and synthesis. MOFs as an important class of porous materials is widely used in gas adsorption/separation,[53,54] catalysis,[55] proton conduction[56] and drug delivery.[57] The porous structure of MOFs is also beneficial both to Li/Na-ion transfer and to the reversible insertion/extraction. For this reason, MOFs and their analogues are employed to modify the microstructure of cathode materials for batteries. This section focuses on the major advances that have been achieved since 2009. We describe the roles of four kinds of MOFs and of their analogues as cathode materials in enhancing the electrochemical performances of Li/Na-ion batteries.

2.1. Metal organic-phosphate open frameworks (MOPOFs)

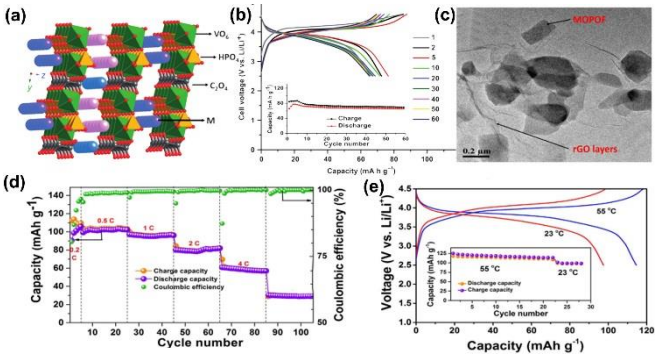

Figure 1. (a) Packing pattern of $K_{2.5}[(VO)_2(HPO_4)_{1.5}(PO_4)_{0.5}(C_2O_4)]$ viewed along the a axis. Green VO_6 octahedra, orange PO_4 tetrahedra, black oxalato C atoms, purple K1, pink K2, blue K3. Hydrogen atoms are omitted for clarity. (b) Galvanostatic charge-discharge profiles of $K_{2.5}[(VO)_2(HPO_4)_{1.5}(PO_4)_{0.5}(C_2O_4)]$ at 0.3 C in the voltage window of 2.5-4.6 V and cyclability (inset). (c) TEM image of the composite showing the MOPOF nanoplates embedded in rGO layers (scale: 200 nm). (d) Rate capability studies of rGO/$K_2[(VO)_2(HPO_4)_2(C_2O_4)]$ at current rates of 0.2, 0.5, 1, 2, 4 and 5 C. (e) Charge-discharge profiles of rGO/$K_2[(VO)_2(HPO_4)_2(C_2O_4)]$ at high temperature (55 °C) a current rate of

0.2 C. The inset figure shows the cycle performance at 55 °C [Reprinted with permission from Ref. [58, 60]. Copyright 2012, Wiley. Copyright 2014, Nature.].

Metal organic-phosphate open frameworks (MOPOFs) are hybrid materials with multidimensional architectures constructed from transition metal phosphates cross-linked by organic linkers, which in turn can encapsulate a diverse range of alkali ions (Li^+, Na^+ and K^+) between the layers.[58,59] Furthermore, the coexistence of the organic oxalate and inorganic phosphate anions in MOPOFs is expected to enhance the redox reaction of the transition-metal ions. In this area, a series of systematic researches were carried out by Vittal groups.

The first MOPOFs used as a cathode for LIBs was $K_{2.5}[(VO)_2(HPO_4)_{1.5}(PO_4)_{0.5}(C_2O_4)]$.[58] The single-crystal structure of the sample synthesized by a hydrothermal process involves the asymmetric unit, i.e., one formula unit $K_{2.5}[(VO)_2(HPO_4)_{1.5}(PO_4)_{0.5}(C_2O_4)]\cdot 4.5H_2O$ (Figure 1a). $K_{2.5}[(VO)_2(HPO_4)_{1.5}(PO_4)_{0.5}(C_2O_4)]$ showed reversible Li^+ intercalation/extraction. The initial discharge capacity of this material is only about 80 mA h g^{-1}, and this is not satisfying (Figure 1b). In spite of the disadvantage, the MOPOFs could still be a potential alternative cathode material for LIBs, even for SIBs, owing to its remarkable porous structure, synthetic simplicity and low-cost. Vittal succeed in improving the electrochemical performance of $K_2[(VO)_2(HPO_4)_2(C_2O_4)]$.[60] Reduced graphene oxide (rGO) is known to exhibit excellent electronic conductivity, two dimensional structure, high surface area and chemical stability. The rGO/$K_2[(VO)_2(HPO_4)_2(C_2O_4)]$ nanocomposites were

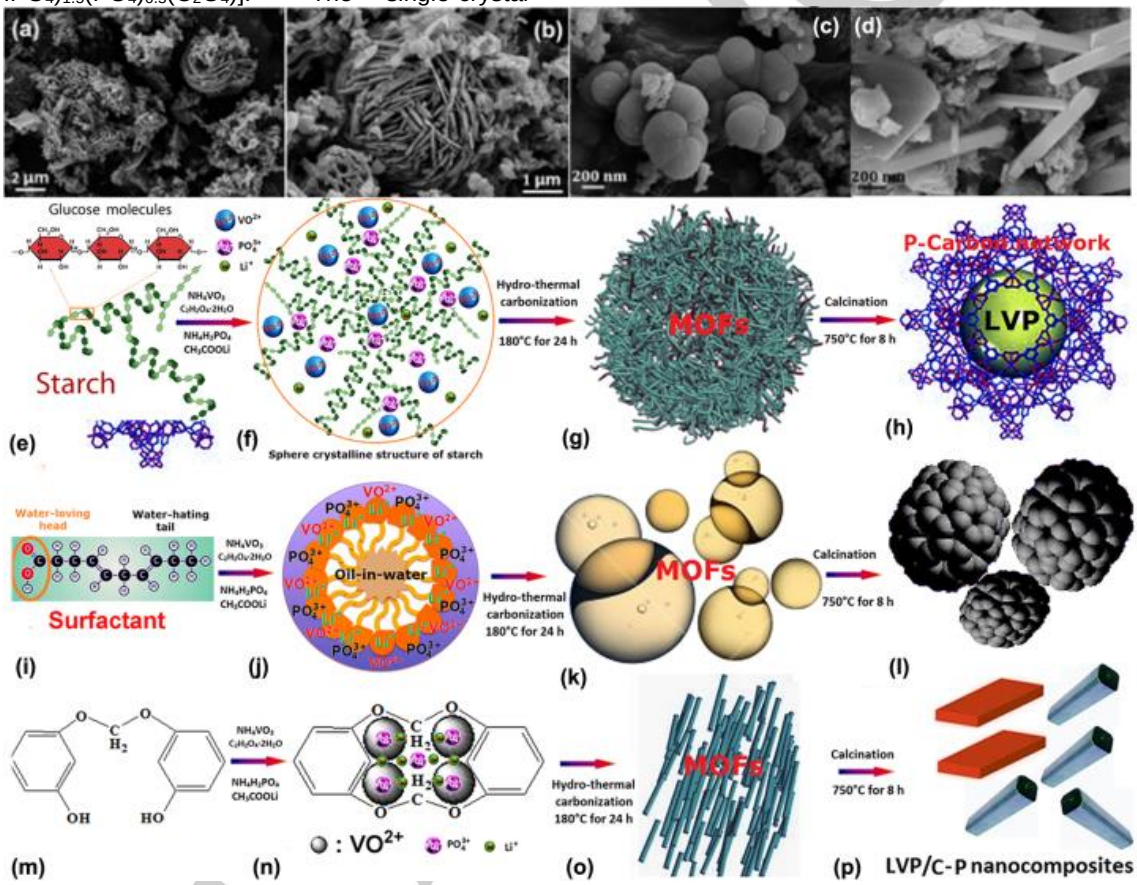

Figure 2. (a-d) Multi-scale structures of the $Li_3V_2(PO_4)_3$/P-C samples characterized by SEM. (e-p) Possible forming mechanism of the $Li_3V_2(PO_4)_3$/P-C nanocomposites with different morphologies. Schematic formation diagrams of (e-h) flower-like structure, (i-l) spheroidal foam structures and (m-p) prism structures. [Reprinted with permission from Ref. [63]. Copyright 2017, Elsevier.].

synthesized by coating rGO layers on $K_2[(VO)_2(HPO_4)_2(C_2O_4)]$ particles (Figure 1c). This strategy is effective for enhancing both initial discharge capacity and rate performance (Figure 1d), since rGO coating layers increase the electronic conductivity of cathode materials, reduce the concentration of electrons on the surface of the cathode, and keep the MOF structure stable, especially at relatively high temperature (e.g., 50 °C). The discharge capacity is 110 mA h g^{-1} after 25 cycles at a current rate of 0.2 C and a temperature of 55 °C (Figure 1e).

In the potassium-containing MOPOF framework, Li^+ ion intercalation occurs after K^+ ion extraction. Since the ionic radius of K^+ is larger than that of Li^+, the ion transfer dynamics and specific capacity are limited. Considering this drawback, a lithium-containing MOPOF material, $Li_2(VO)_2(HPO_4)_2(C_2O_4)\cdot 6H_2O$, was synthesized by Vittal's group.[61] Although the electrochemical properties of this material are not particularly satisfying, it is still worth being tested. The above-mentioned methods have a common feature, i.e., the calcination process is skipped, enable cost-

effective synthesis. However, both the electrochemical performances and the structure stability of the MOPOF cathode are not ideal. Then, Vitall et al synthesized the carbon coated $Li_3V_2(PO_4)_3$ from the $Li_2(VO_2)(HPO_4)_2(C_2O_4)\cdot 6H_2O$ precursor and subsequently subjected it to calcination.[62] The prepared samples were characterized by XRD quantitative rietveld refinement, N_2 adsorption-desorption measurements and electrochemical tests. The results indicate that these samples exhibit stable rate performances, e.g., the discharge capacity obtained at the current rates of 20 C reaches 56 mA h g^{-1}. This study demonstrated that the calcination process was a crucial factor to ensure both structural stability and good rate performance.

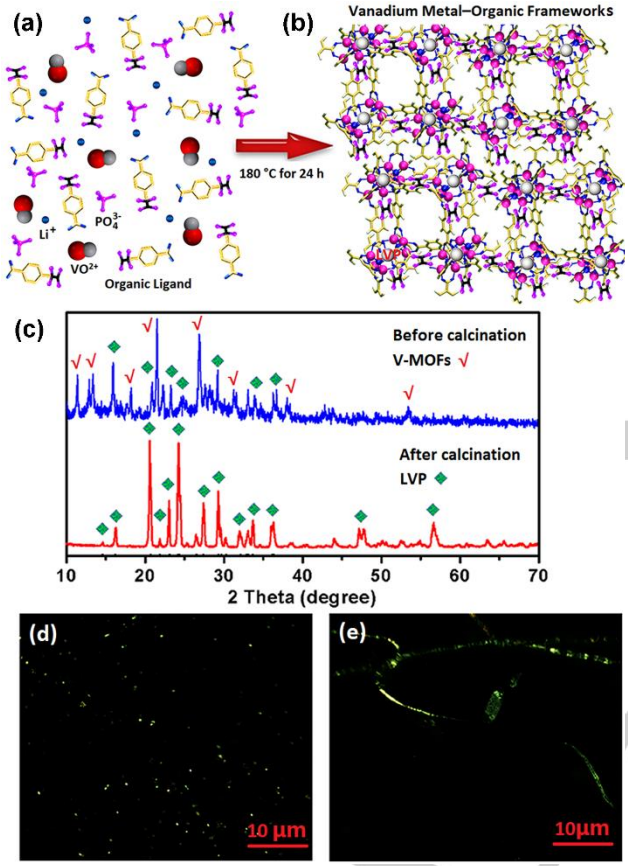

Figure 3. (a, b) Schematic illustration of the prepared process for V-MOFs precursors via hydrothermal carbonization. (c) XRD patterns of the obtained samples before and after calcination. (d, e) Polarizing optical microscopy images of the samples before and after the hydrothermal carbonization under the orthogonal polarization. [Reprinted with permission from Ref. [63]. Copyright 2017, Elsevier.].

Wang, et al. synthesized $Li_3V_2(PO_4)_3$/phosphorus-doped carbon (LVP/P-C) nanocomposites with multilevel structures using vanadium metal-organic frameworks (V-MOFs) as precursor by subsequent calcination.[63] The formation mechanism of polymorphological samples can be explained through Figures 2a-p. Flower-like structure (Figure 2b) is created through self-assembly of starch template as shown in Figures 2e-h. The functional groups of glucose chain in starch molecules are combined with VO^{2+}, PO_4^{3-} and Li^+ by electrostatic adsorption. Subsequent to V-MOF formation during the hydro-thermal carbonization process, a flower-like structure can be obtained upon calcination process. Figures 2i-l illustrate a possible formation mechanism of hierarchical spherical structure (Figure 2c) via self-assembly of surfactant templates. When the surfactant concentration is higher than the critical micelle concentration (CMC), the oil-in water micelles are formed by the surfactant molecule self-assembling, and VO^{2+}, PO_4^{3-} and Li^+ are adsorbed on the micelle surface by water-loving head. The different micelle particles are connected by VO^{2+} and PO_4^{3-}. The oil-in-water micelles are transformed into V-MOFs through the hydrothermal carbonization, leading to formation of the hierarchical spherical structures during the subsequent calcination process. The possible formation mechanism of prism structures (Figure 2d) is described in Figures 2m-p. "Cage" structure could be generated after a two-step semi-condensation polymerization between resorcinol and formaldehyde. VO^{2+}, PO_4^{3-} and Li^+ could be locked in this "cage", in which the $Li_3V_2(PO_4)_3$ particles grow and stack. The V-MOFs were obtained by the hydro-thermal carbonization and then assemble into the different prism structures during the subsequent sintering process.

The topological structure of the V-MOF precursor can be seen in Figures 3a-b. The reaction involves the reactants (metal ions and phosphate) and the organic linkers, which form a complex structure as the nucleation center for the growing structure. The liquid crystal phases were transformed into V-MOF crystals after the hydrothermal carbonization at 180 °C for 24 h, as proven by the interference color change in Figures 3d-e. The crystal structure of V-MOFs was confirmed by XRD patterns (Figure 3c). Wang, et al. argue that the multilevel structure could provide more buffer space for volume change of the cathode materials and offer more active reaction sites during the charge/discharge processes. So the LVP/P-C sample exhibits a discharge capacity of 65 mA h g^{-1} at 10 C with 90% capacity retention after 1100 cycles. This result further verifies that the structural stability and the rate performance could be improved via calcination process.

2.2. Prussian blue and its analogues

Prussian blue (PB) and its analogues (PBAs) could be described by a general chemical formula $A_xM_1[M_2(CN)_6]_{y\cdot 1-y}\cdot nH_2O$,[64] where A is alkali metal, M1 and M2 are transition metal ions, 0<x<2, y<1. It is known that the general criteria for an ideal cathode material for LIBs or SIBs include the following aspects: (a) containing valence variable element so as to ensure the presence of reversible redox reactions in batteries; (b) bearing alkali metal ions in order to ensure the ion exchange between cathode and anode electrodes during charging and discharging process; (c) possessing high structural stability, which is crucial for the high-rate and long-cycling performances; (d) exhibiting high electronic conductivity and high ion diffusion coefficient that are important for enhancing the transfer efficiency of electrons and ions during charging and discharging; (e) having potential for commercial applications[65-67] and cost-effective production; (f) requiring raw materials that are abundant in nature. PB and PBAs basically meet the above-mentioned requirements.

It was reported that the pristine PB (KFeFe(CN)6) shows a much lower coulombic efficiencies.[32,68] PB has a cubic framework with Fe(II) and Fe(III) on alternate corners of a cube of corner-shared octahedra bridged by linear $(C\equiv N)^-$ anions (as shown in Figure 4a). Goodenough et al. investigated the electrochemical performances of $KMFe(CN)_6$ with M = Mn, Fe, Co,

Ni, and Zn in SIBs.[32] But these systems cannot give high discharge capacity and Coulombic efficiency in organic electrolyte. Cui et al explored the electrochemical performances of copper hexacyanoferrate[69] and nickel hexacyanoferrate[70] in aqueous electrolyte. These systems show enhanced Coulombic efficiency, high rate and long-life performances. Goodenough et al further improved the electrochemical performances of PB and PBAs by substituting Na^+ for K^+. $Na_{1.72}MnFe(CN)_6$ was synthesized by Goodenough et al, which showed a reversible discharge capacity of 134 mA h g^{-1} at 0.05 C with 89.6% capacity retention after 30 cycles.[71] They also found that there is a positive correlation between sodium ion concentration and electrochemical performances. Following their work, sodium rich PB or PBAs were extensively studied. Huang et al[72] reported that Na-rich $Na_{1.7}FeFe(CN)_6$ had a discharge capacity of 120.7 mA h g^{-1} at a current density of 200 mA g^{-1}, and showed 73.6 mA h g^{-1} even at 1200 mA g^{-1}. Chou et al[73] synthesized Na-enriched $Na_{1.56}FeFe(CN)_6{\cdot}3.1H_2O$ sample by a facile one step method, which showed a high discharge capacity of 100 mA h g^{-1} and an excellent capacity retention of 97% after 400 cycles. Wang et al.[74] reported a novel acetic acid induced Na-rich $Na_{3.27}Fe_{0.35}[Fe(CN)_6]{\cdot}0.85H_2O$ nanocubes, which exhibited a reversible capacity of 103 mA h g^{-1} at a current density of 25 mA g^{-1} and an 87% capacity retention after 100 loops at the current density of 100 mA g^{-1}.

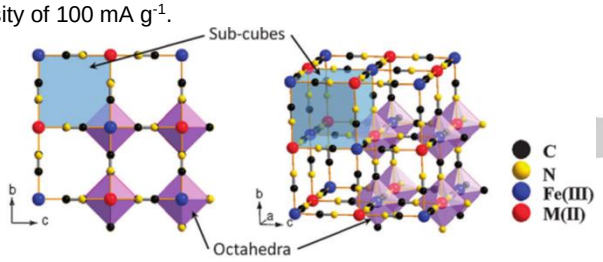

Figure 4. Framework of Prussian blue analogues. [Reproduced from Ref. [32] with permission from The Royal Society of Chemistry.].

It is found that the $[Fe(CN)_6]$ vacancies occupied by coordinating water in PB and PBAs may induce lattice distortion (as shown in Figure 5a) and even collapse of the crystal framework during Na^+ insertion/extraction.[75] Goodenough et al[76] prepared a rhombohedral Prussian white (R-$Na_{1.92}Fe[Fe(CN)_6]$) with few $[Fe(CN)_6]$ vacancies as air-stable cathode for SIBs, and thereby avoid the lattice distortion and crystal framework collapse caused by $[Fe(CN)_6]$ vacancies. The obtained sample showed a long cycle life and good rate capability. Zuo et al. [77] synthesized a high crystallinity MnCoNi-co-doped PBA composite cathode with less $[Fe(CN)_6]$ vacancies and coordinated water by a citrate-assisted controlled crystallization process. This composite cathode exhibited a reversible capacity of 111 mA h g^{-1} at 1 C and retained a capacity retention of 78.7% after 1500 cycles for SIBs. Ong et al.[78] elucidated the effect of lattice water on the phase stability and the voltage profile. That is, the presence of lattice water can raise the voltage and can act as pillars to reduce the volume change during the charging/discharging process. On the other hand, a reduced graphene oxide modified Prussian blue without coordinating water was first synthesized by Ma et al.[79] An high discharge capacity of 149.7 mA h g^{-1} was obtained at 200 mA g^{-1} from 2.0 V to 4.0 V with capacity retention of 91.9% after 500 cycles. Jiang et al[64] developed a facial in-situ synthesis method to fabricate PB/C composites, which showed an unprecedented rate performance and excellent cycling stability, e.g., the discharge capacity of 77.5 mA h g^{-1} at 90 C (Figure 5c). Even after 2000 cycles at 20 C. These composites exhibit 90 mA h g^{-1} with 90% capacity retention (Figure 5b). This synthetic method is simple and cost-effective, and is believed to have potential for commercialization. Moreover, there also are some other studies to develop high performance PB by controlling pore size[80] and morphology.[81]

In recent years, some researchers focused on the development of PB- or PBAs-based full batteries. Ji et al.[82] assembled the full-cell with Ni-Fe PBAs cathode and the Ni-Fe PBAs derived $Ni_{0.67}Fe_{0.33}Se_2$ anode. This full-cell showed a remarkable Na-ion storage capacity of 302.2 mA h g^{-1} at 1.0 A g^{-1}. Organic carbonate electrolytes are widely used in LIBs and SIBs. However, due to their safe and economic problems, SIBs containing aqueous electrolytes have received much attention.[83,84] Varzi et al.[85] assembled SIBs involving $Na_2MnFe(CN)_6$ cathode and $NaTi_2(PO_4)_3$ anode and aqueous electrolytes. This battery displayed depressed initial discharge capacity of 57 mA h g^{-1} at 0.1 A g^{-1} and low average discharge voltage of 0.82 V. Okada et al.[86] developed a high discharge voltage (2 V) full cell that consist of sodium manganese hexacyanoferrate cathode, potassium manganese hexacyanochromate anode and highly concentrated $NaClO_4$ aqueous electrolyte. This modification strategy can effectively enhance the energy density and power density of SIBs with aqueous electrolytes.

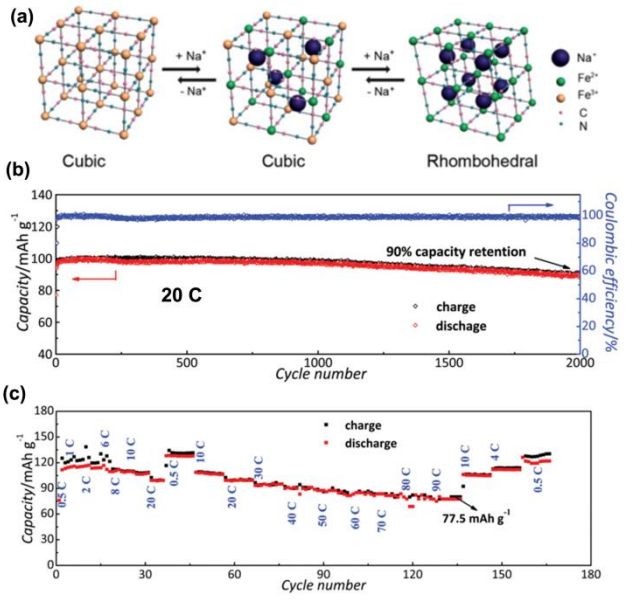

Figure 5. (a) Schematic illustration of the redox mechanism of PB and PBAs. (b) Cycling performance of Prussian blue/C at a rate of 20 C in the potential window of 2.0-4.0 V vs Na/Na^+. (c) Rate capability of Prussian blue/C at current rates ranging from 0.5 to 90 C. [Reproduced from Ref. [60] with permission from The Royal Society of Chemistry. Reprinted with permission from Ref. [64]. Copyright 2016, Wiley.].

2.3. Materials Institut Lavoisier (MIL)

Materials Institut Lavoisier (MIL) is a type of MOF materials developed by Institut Lavoisier de Versailles. MIL possesses large pores and high porosity, in addition, the sizes of the pores is easy

to be modulated.[87] These characteristics of MIL can be used to modify their electrochemical performances. Therefore, numerous studies were carried out to explore the potential of MIL materials to be used as cathode for batteries.

Férey et al[88] reported MIL-53(Fe)·H_2O ($[Fe(OH)_{0.8}F_{0.2}(O_2CC_6H_4CO_2)]\cdot H_2O$) as cathode materials for LIBs. They found that the number of inserted Li atoms per formula unit is only 0.6, and the density of MIL-53(Fe)·H_2O is lower (1.7 g cm^{-3}) than that of other cathode materials. Moreover, the electronic conductivity of MIL-53(Fe)·H_2O is poor. These shortcomings are a barrier for MIL-53(Fe) to be used as cathode materials. In order to further improve the capacity of MIL-53(Fe) materials, Férey et al used MIL-53(Fe) to adsorb the electro-active molecules (1,4-benzoquinone). 1,4-benzoquinone can act as redox mediator to enhance the electronic transfer efficiency in the MIL-53(Fe) materials. Theoretically, 1,4-benzoquinone can accept two electrons per molecule, and thereby increases the theoretical specific capacity of the composite cathode materials.[89] Unexpectedly, quinone can partially dissolve into the electrolytes, and reversibly react only with 0.5 Li rather than with the 2 Li. The discharge capacity retention becomes worse after multiple cycles. They discovered an interesting phenomenon, i.e., the quinone molecules and hydrophilic part of the octahedral chain are linked by π-π interactions (Figure 6). Optimizing the π-π interactions can result in phase transition, which has an impact on both lithium and hydrogen storage. They also explored another Fe based MIL that was named as MIL-68(Fe).[90] However, the electrochemical performances of MIL-68(Fe) are inferior to MIL-53(Fe).

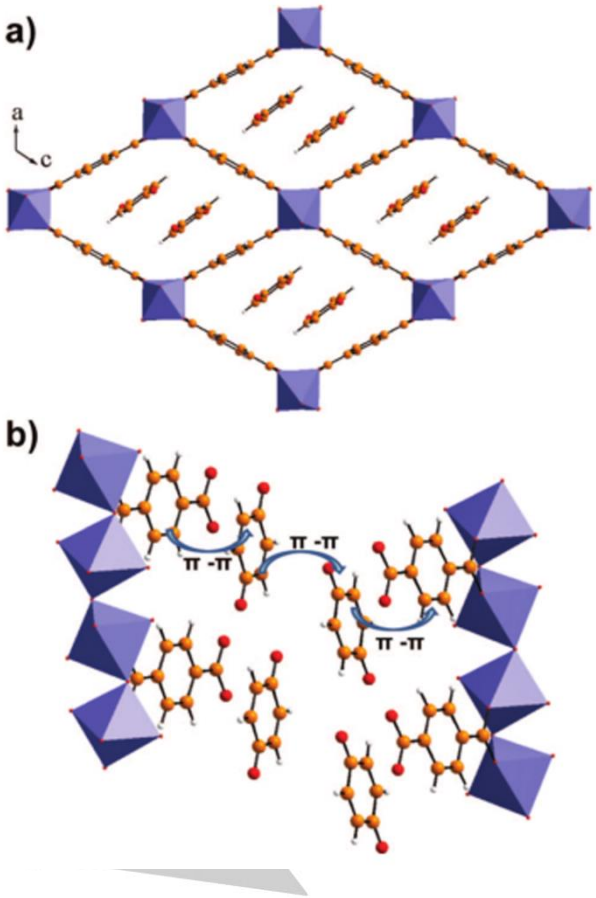

Figure 6. Drawing of the unit MIL-53(Fe)-quinone structure with in (a) and (b), different views showing the global and detailed interactions between the host quinone molecules and MOF linkers. [Reprinted with permission from Ref. [89]. Copyright 2009, American Chemical Society.].

Meng et al. also investigated MIL-101(Fe) cathode material, which consists of the carboxylate-bridged trinuclear Fe^{3+} complex with an oxygen-center (Figures 7ab).[91] Its average pore diameter is larger than MIL-53(Fe). The theoretical capacity of MIL-101(Fe) with one lithium insertion per Fe atom is 107.74 mA h g^{-1}. Owing to the irreversible redox reaction (Fe^{2+}/Fe^{3+}) in MIL-101(Fe), the capacity fades after many charging/discharging cycles. Both ex-situ and in-operando X-ray Absorption Spectroscopy (XAS) measurements were conducted to

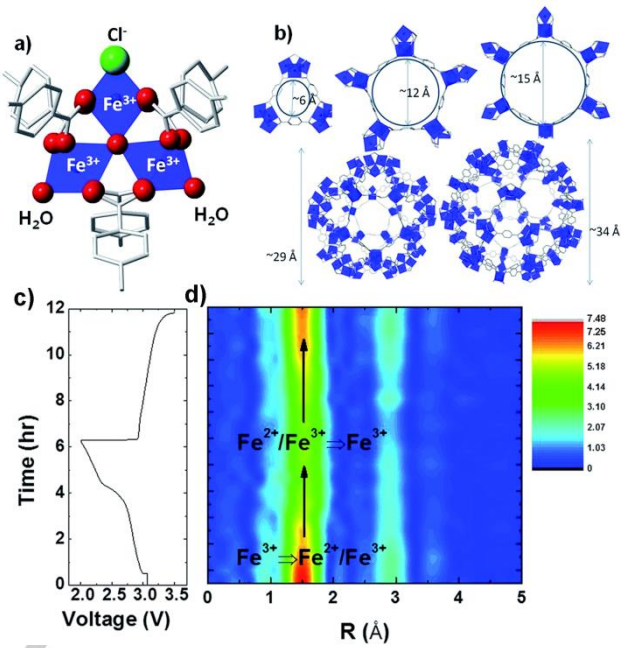

Figure 7. (a) Structure of MIL-101(Fe), blue, Fe; red, O; stick, C; green, Cl; H is omitted for clarity. (b) The windows and pores of MIL-101(Fe) with Cl and O atoms omitted for clarity. (c) Voltage profile with respect to the in-operando XAS scanning time. (d) Contour plot of the EXAFS region versus time that indicates a reversible change in Fe coordination during cycling. [Reproduced from Ref. [91] with permission from The Royal Society of Chemistry.].

investigate the decay mechanism of MIL-101(Fe) cathode. The change of the peak intensity at 1.5 Å is reversible during lithiation/de-lithiation process (Figures 7cd). Meng et al attributed this reversible spectroscopic change to a reversible change in the coordination environment of the nearest neighbors. This result is useful for designing the MIL-101(Fe) cathode materials to improve the reversibility of the Fe^{2+}/Fe^{3+} redox reaction. Férey et al synthesized $[Ni_2(H_2O)_5(TTF\text{-}TC)]\cdot H_2O$ (MIL-136(Ni)) as cathode for LIBs. [92] It turned out that MIL-136(Ni) is inadequate to act as cathode, because of its low Li-ion mobility and redox irreversibility. Recently, Jacobson et al reported a vanadium-based metal organic framework V(O)(bdc) [MIL-47(V)], which delivered superior electrochemical performances.[93] The discharge capacity of MIL-47(V) cathode is 118 mA h g^{-1} at 0.1 C at the voltage window between 1.6 V to 3.5 V. Even when the rate went up to 10 C it also delivered capacity of 40 mA h g^{-1}. Considerable progress has been made in improving discharge

capacity and rate performance for vanadium-based MOFs cathode for LIBs. Other MOF cathodes were also used for LIBs, e.g. K(TTF-TC)H_2 (TTF-TC=tetrathiafulvalenetetracarboxylate)[94] and Cu(2,7-AQDC) (2,7-H_2AQDC=2,7-anthraquinonedicarboxylic acid),[95] but their electrochemical performances were not satisfying. In addtion, MIL-derived cathodes also attract much attention of battery researchers. Kim et al.[96] synthesized FeOF nanoparticles wrapped in graphitic carbon layers, which were *in-situ* prepared from Fe-MIL-88B. This FeOF-based composite cathode showed a reversible capacity of 338 mA h g^{-1} at a current density of 100 mA g^{-1} after 100 cycles. A similar work was also performed by Zhang et al..[97] They used MIL-53 as precursor and self-template to *in-situ* fabricate 3D porous carbon/FeF_3·0.33H_2O composite cathode. This cathode exhibited a capacity of 113 mA h g^{-1} after 300 cycles at 5 C. Even at ultra-high rate of 20 C, the capacity remains 86 mA h g^{-1} yet.

2.4. MOFs coating layer materials

Cathode materials in general suffer from low electron conductivity and large volumetric change during the charging/discharging process. It was found that coating could contribute to overcoming these problems. Carbon-based coating materials provide higher electron conductivity. Metallic oxides usually act as protective layers to avoid the structure collapse of electrode materials caused by volume change.

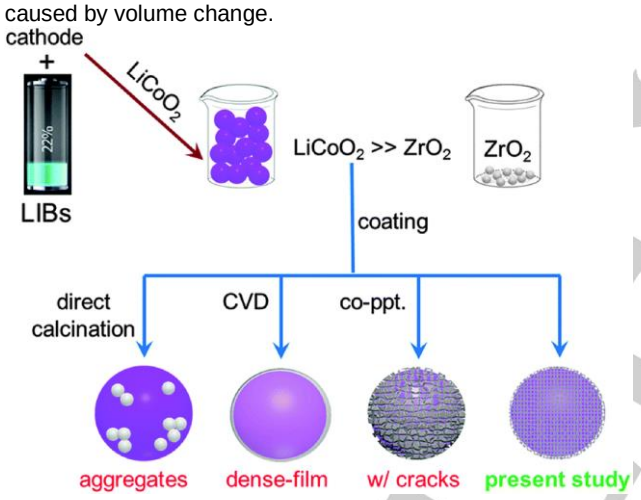

Figure 8. Different routes to coat $LiCoO_2$ (co-ppt denotes co-precipitation) [Reproduced from Ref. [98] with permission from The Royal Society of Chemistry.].

Wang et al[98] reported that metallic oxide coatings derived from MOFs were well-dispersed on the surface of $LiCoO_2$ cathode. This method can avoid several problems, such as aggregates, dense coating, and incomplete and cracked coverages on the surfaces of cathodes, which are caused by direct calcination, chemical vapor deposition (CVD) and co-precipitation (co-ppt), respectively (Figure 8). The cathode coated by MOFs derived metallic oxide deliver excellent rate performance and superior thermal stability. A similar work was carried out by Wang et al., who synthesized a carbonized ZIF-8 coated $LiFePO_4$ by the in situ growth and carbonization of ZIF-8.[99] The discharge specific energy retention rate of this sample is approximately 99% at a rate of 5 C after 200 cycles. Xie et al.[100] reported that $Li_{1.2}Mn_{0.54}Co_{0.13}Ni_{0.13}O_2$ coated by UIO-66-F4 derived ZrO_2 exhibited high discharge capacities of 279 and 110 mA h g^{-1} at 0.1 C and 5 C, respectively. Besides, MOFs-derived carbon was also used as coating layer for $Li_3V_2(PO_4)_3$ cathode material.[101] The composites cathode showed a superior electrochemical stability with excellent reversible capacities of 113.1 and 105.8 mA h g^{-1} at the rate of 0.5 C and 1 C, respectively, after 1000 loops. These simple but effective treatments could also be employed in anode majorization.[102-104]

Wang et al[98] synthesized the MOFs coated electrode materials via secondary calcination. Although these materials exhibit excellent electrochemical performance, the secondary calcination can cause more energy consumption. Dou et al discovered and synthesized two kinds of two dimensionally connected MOFs-$Ni_3(HIB)_2$ and $Cu_3(HIB)_2$ (HIB=hexaiminobenzene).[105] The black samples of $M_3(HIB)_2$ (M=Ni, Cu) can be acquired from reactions of HIB·3HCl with ammoniacal solutions of $Ni(NO_3)\cdot 6H_2O$ or $CuSO_4\cdot 5H_2O$ in mixtures of water and dimethylsulfoxide heated at 60 °C in air for two hours (Figure 9b). It was found that the Fermi energy of $M_3(HIB)_2$ (M=Ni, Cu) locates in a partially filled delocalized band, and hence, these materials show metallic behavior and become bulk electrical conductors. The electronic conductivity of $Cu_3(HIB)_2$ is close to 1300 S m^{-1} at 300 K under vacuum, which is 10 orders of magnitude higher than $Li_3V_2(PO_4)_3$ (10^{-7} S m^{-1}). Otherwise, the electronic conductivity of the $M_3(HIB)_2$ (M=Ni, Cu) increases linearly with increasing temperature (Figure 9c). The authors inferred that the path of electron transport could be along the skeleton of $M_3(HIB)_2$ (M=Ni, Cu) as shown in Figure 9a. These kinds of metallic MOFs should be promising candidates as electrode coating layers used for batteries due to their excellent electronic conductivity.

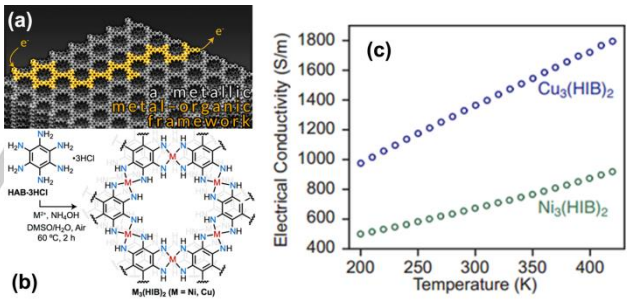

Figure 9. (a) The electronic conductive mechanism and structure of $M_3(HIB)_2$. (b) Synthesis of $Ni_3(HIB)_2$ and $Cu_3(HIB)_2$. (c) Variable-temperature electrical conductivity of pressed pellets of $M_3(HIB)_2$ measured by the van der Pauw method under vacuum. [Reprinted with permission from Ref. [105]. Copyright 2017, American Chemical Society.].

Combining MOFs with other components of cathode is still a challenge. As described above, combination of MOFs can be carried out with or without calcination. Inevitably, MOF-derived cathodes without calcination can partially dissolve into organic electrolyte, and this is detrimental to the specific capacity. Moreover, the structural stability of MOFs materials is far from being satisfying, and thus the rate performance is limited. Calcination is a useful process to enhance the structural stability, however, it would damage the structure of MOFs.

3. MOFs-derived cathode materials for Li-S/Li-Se batteries

Traditional cathode materials, such as $LiCoO_2$, $LiFePO_4$ and $LiMn_2O_4$, suffer from the theoretical limit of their specific capacity, and thus cannot enable highly effective power storage and discharge required by a sustainable modern society. The theoretical specific capacity and energy density of Lithium-sulfur (Li-S) batteries are 1672 mA h g^{-1} and 2600 W h kg^{-1},[108,109] respectively. It is believed that Li-S batteries are the most promising candidates for next generation of commercial batteries. Furthermore, sulfur is cheap and environment friendly. The reaction mechanism of Li-S batteries[110] is described as follow:

$$S_8 + 2e^- \rightarrow S_8^{2-} \quad (1)$$

$$S_8^{2-} \leftrightarrow S_6^{2-} + \frac{1}{4}S_8 \quad (2)$$

$$2S_6^{2-} + 2e^- \leftrightarrow 3S_4^{2-} \quad (3)$$

$$3S_4^{2-} + 2e^- \leftrightarrow 4S_3^{2-} \quad (4)$$

$$2S_3^{2-} + 6Li^+ + 2e^- \leftrightarrow 3Li_2S_2 \quad (5)$$

$$Li_2S_2 + 2Li^+ + 2e^- \leftrightarrow 2Li_2S \quad (6)$$

From the illustration of Li-S batteries (Figure 10a) and the above equations, we can find that there are many parallel redox reactions during charging and discharging processes. The voltage platforms corresponding to different redox reactions are described in Figure 10b. It is clear that the redox intermediate polysulfides (Li_2S_x) are transfer medium of ions for Li-S batteries. However, Li_2S_x are highly soluble in the electrolyte, resulting in the loss of capacity.[29,111] Moreover, the sulfur cathode structure could collapse because of its intense volume changes during the charging/discharging process, leading to dramatic capacity fading. Furthermore, the insulating properties of sulfur and polysulfides are a serious problem to be solved to develop high-performance Li-S batteries.[112-114] Encapsulation of sulfur is an effective strategy to reduce the volume change and restrain the shuttle effect. Embedding sulfur in MOFs or MOFs-derived carbon are two approaches to achieve this objective.[115-117]

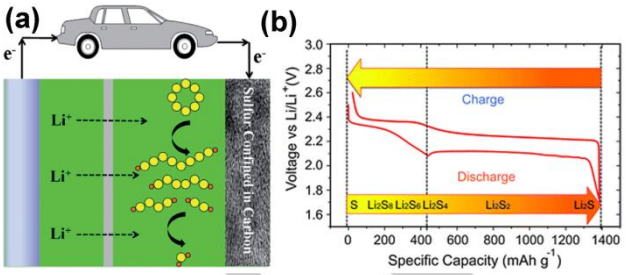

Figure 10. (a) Illustration of the Li-S batteries (yellow is sulfur and orange is lithium). (b) The voltage profile and chemistry of sulfur cathode in the organic electrolyte. [Reproduced from Ref. [106,107] with permission from The Royal Society of Chemistry.].

3.1. Sulfur/MOFs hybrid cathode materials for Li-S batteries

MOF materials are characterized by their high porosity and high specific surface area. The porous structure can host sulfur and thereby limit the volumetric change. Tarascon et al prepared chromium metal organic framework (MIL-100(Cr)) as host material for sulfur impregnation.[118] The same procedures were also applied to other hosting materials such as mesoporous carbon and SBA-15. It was found that MIL-100 (Cr) material could be used to improve capacity retention.[118] The pore size of MOFs is an important parameter for judging the suitability of MOFs as a hosting material of sulfur. Lin et al[119] demonstrated that S_8 was not able to enter the cavities of ZIF-8 since the channels between cavities (0.34 nm) is smaller than the molecular diameter of S_8 (0.68 nm), whereas HKUST-1 and MOF-5 could easily accommodate S8. However, this does not mean that ZIF-8 cannot be used as a sulfur hosting material, as it can accommodate other forms of sulfur (e.g., S_6, S_4 and S_2). Li et al carried out a detailed work on four representative MOFs,[120] i.e., MIL-53 (Al) (with 1D channels), NH_2-MIL-53 (Al) (with amine functionality), HKUST-1 (with unsaturated metal sites) and ZIF-8 (cage type pores with small entrance) as shown in Figures 11a and b. By comparison, ZIF-8 was found to possess the maximum capacity retention ratio (76%). However, those framework channels larger than 0.68 nm cannot immobilize sulfur. However, according to Li et al, the internal environment (such as Lewis acidic centers) could improve the immobilization of sulfur. Siegel et al confirmed this effect,[121] and demonstrated that the coordinatively unsaturated metal sites in MOFs could suppress the dissolution of polysulfide intermediates by chemical adsorption. Liu et al.[122] explored a manganese cluster-based MOF, which could effectively capture polysulfides. Therefore, this composite cathode displayed a high discharge capacity of 990 mA h g^{-1} after 200 cycles at 2 C. Cai et al.[123] designed a S@Cu-MOF (Cu-TDPAT) composite cathode with dual functional binding sites (i.e., Lewis acid and base sites) for Li-S batteries. Owing to the synergistic effects of nanoporous Cu-MOFs and the funcational binding sites, the composite exhibited excellent rate and cycling performances (that is, 745 mA h g^{-1} after 500 loops at 1 C).

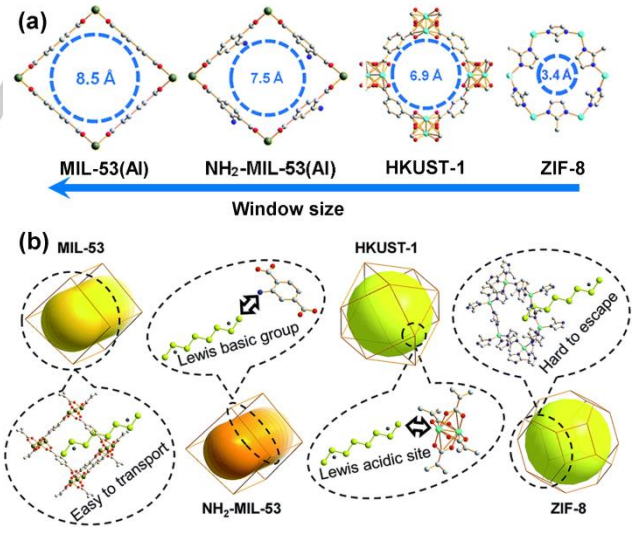

Figure 11. (a) Schematic of the largest apertures of the four MOFs. (b) Schematic of the four MOFs and their unique characteristics. [Reproduced from Ref. [120] with permission from The Royal Society of Chemistry.].

Graphene and reduced graphene oxide can endow MOFs high electrical conductivity and high mechanical strength. According to Chen et al,[124] MIL-101 (Cr)/sulfur composite could

be wrapped by graphene, and thereby the capacity of 809 mA h g^{-1} was maintained after 134 cycles at 0.8 C rate with a 95% capacity retention. As a comparison, MIL-101 (Cr)/sulfur composite without graphene wrapping retains a much lower capacity of 695 mA h g^{-1} after 100 cycles at a lower current density of 0.1 C. Hao et al found thermal exfoliation of MOFs into multilayer graphene stacks.[125] This method can be used to fabricate multilayer graphene with uniform morphology, highly polarized carbon surface and hierarchical porous structures. The method not only limits the dissolution of polysulfide, but also promotes the electron and ion transfer. However, high preparation cost of graphene hinders the large-scale applications of this method. Carbon nanotubes (CNTs), like graphene, possess superior electronic conductive performance and mechanical property. Moreover, the production cost of CNTs is much lower than that of graphene. Utilizing these advantages of CNT, Cao et al.[126] synthesized a mutually embedded ZIF-8@CNTs hybrid networks as sulfur host materials for Li-S batteries. The S@ZIF-8@CNTs composite cathode exhibited a high initial discharge capacity (1380 mA h g^{-1} at 0.1 C) and excellent long-term cycling stability (750 mA h g^{-1} after 500 cycles at 1C).

3.2. Sulfur/MOFs derived carbon cathode materials for Li-S batteries

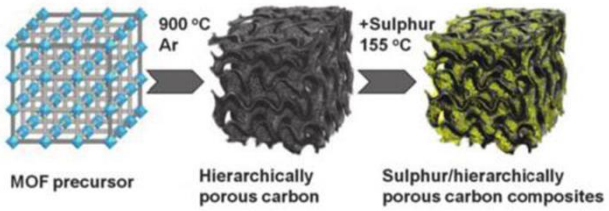

Figure 12. Scheme of sulphur-hierarchical porous carbon composite preparation. [Reproduced from Ref. [129] with permission from The Royal Society of Chemistry.].

The MOF derived carbon originates from the carbonization of MOFs in inert atmosphere. The carbonization of MOFs was often used to synthesize porous carbon.[127,128] The MOF derived carbon as a sulfur host has some advantages, e.g., lower solubility and higher structural strength compared to pure MOFs. The sulfur/MOF derived carbon is prepared by evaporation of sulfur into the MOF derived carbon by controlling temperature (as shown in Figure 12). However, carbonization of MOFs may destroy the inherent structures of MOFs, so the pore size and structure of MOFs derived carbon cannot be precisely controlled. Furthermore, the pyrolysis of organic ligands makes MOFs derived carbon be not able to adsorb polysulfide.

Kumar et al.[129] used hierarchical porous carbon (HPC), prepared by carbonizing MOFs, as host for encapsulating sulfur in Li-S batteries. It was found that mesopores and micropores were conducive to improve initial discharge capacities and cycle stability of Li-S batteries, respectively. A similar work was reported by Zhang et al..[130] Three-dimensional HPC nanoplates acquired from one-step pyrolysis of MOF-5 was used as sulfur hosts. This cathode composite delivered an initial discharge capacity of 1177 mA h g^{-1} at 0.1 C. Even at 0.5 C, the retention capacity could still reach 730 mA h g^{-1} after 50 cycles with the Coulombic efficiency of 97%. Zhang et al.[131] designed HPC/sulfur composites with an one-dimensional French fries like structure, which showed a discharging capacity of 763 mA h g^{-1} at a rate of 2 C. Fabricating multilevel structures is considered as an ideal method to improve rate and cycling performances of cathode materials for Li-S batteries. MOF-derived porous carbon anchored on graphene sheets serving as a sulfur host matrix was explored by Sun et al.,[132] which displayed an initial discharge capacity of 1372 mA h g^{-1} at 0.1 C and a remaining capacity of 608 mA h g^{-1} after 300 cycles at 1 C. Nitrogen-doped MOFs-derived micropores carbon was synthesized by Yin et al..[133] N-doping in MOFs-derived micropores carbon not only facilitates the fast charge transfer, but also improves the interaction between carbon and sulfur. So these materials displayed the excellent rate performance of 632 mA h g^{-1} at 5 A g^{-1}.

3.3. Selenium/MOFs derived carbon cathode materials for Li-Se batteries

The working principle of the lithium-selenium (Li-Se) batteries, which was first reported by Amine et al.,[134] is similar to that of Li-S batteries. The redox reaction during charging/discharging process can be described by the equation:

$$Se + 2Li^+ + 2e^- \leftrightarrow Li_2Se \qquad (7)$$

The theoretical values for both gravimetric capacity and volumetric capacity of Li-Se batteries were found to be 678 mA h g^{-1} and 3253 mA h cm^{-3}, respectively.[135,136] These values are high enough to realize commercialization of Li-Se batteries. In addition, Li-Se batteries show high working voltage, which may result in high volumetric energy density. It was found that Li-Se cathode had a better electrochemical activity and weaker shuttle effect than Li-S cathode.[137] Since there is similarity in working principle between Li-S and Li-Se batteries, the modified methods of Li-S batteries are also applicable to Li-Se batteries.

Designing second building units (SBU) by combining Se and conductive agents can reduce the solubility of polyselenides in electrolytes.[138,139] Xu et al. fabricated hierarchically porous carbon microcubes (CMCs) composed of bubbles derived from MOFs[140] (Figures 13a and d). Selenium was impregnated in CMCs, and thereby a kind of Se/CMCs composite cathode was obtained, which exhibited a high reversible capacity of 425.2 mA h g^{-1} after 100 cycles at 0.2 C. The synthesis mechanism of Se/CMCs is similar to that of S/HPC, i.e., carbonization of MOFs and the embedding of Se (Figure 13g). Normally, Se is dispersed into porous materials through diffusion or infiltration (Figure 13h). Selenium can be encapsulated into MOFs-derived hierarchically porous carbon spheres (MHPCS).[141] Hollow carbon bubbles (about 20 nm) were coated with about 5 nm thick shells to form MHPCS (Figures 13b and e). The Se/MHPCS composites exhibited the excellent cycling stability of >500 cycles at 0.5 C with a capacity retention of 60%. Even the rate rised up to 1 C, the discharge capacity could be maintained at 200 mAh g^{-1} after 1000 cycles. Yin et al.[142] fabricated the nitrogen doped carbon sponges (NCS) via carbonization of MOFs, and then obtained the Se/NCS composite cathode by impregnating Se into NCS (Figures 13c and f). This cathode delivered a surplus capacity of 443.2 mA h g^{-1} after 200 cycles at 0.5 C with a capacity retention of 93.8%. Moreover, this cathode showed an infusive rate performance, and the discharge capacity of 286.6 mA h g^{-1} at the high rate of 5 C. Yin et al. attributed the superior cycling and rate

performances both to the hierarchically porous structures and to the nitrogen doping that increased the electric conductivity of matrix materials. The porous structures can absorb electrolyte to promote lithiation of selenium, and the channels can facilitate the transfer of lithium selenide. Song et al.[143] fabricated a HPC/Se composite cathode with ZIF-8 derived core and ZIF-67 derived shell. Benefiting from the restrictive effect of hierarchical porous structure, selenium and polyselenides were rarely dissolved into the electrolyte. For this reason, HPC/Se composite cathode delivered a reversible capacity of 555 mA h g^{-1} after 150 cycles at 0.2 C, even at the high rate of 1 C, the remaining capacity still reaches 432 mA h g^{-1} after 200 cycles. Furthermore, Su et al. emdedded Se clusters in HPC derived from a zinc-glutamate MOF for advanced sodium storage.[144] This composite cathode displayed a high discharge capacity of 612 mA h g^{-1} after 200 cycles at 0.2 C.

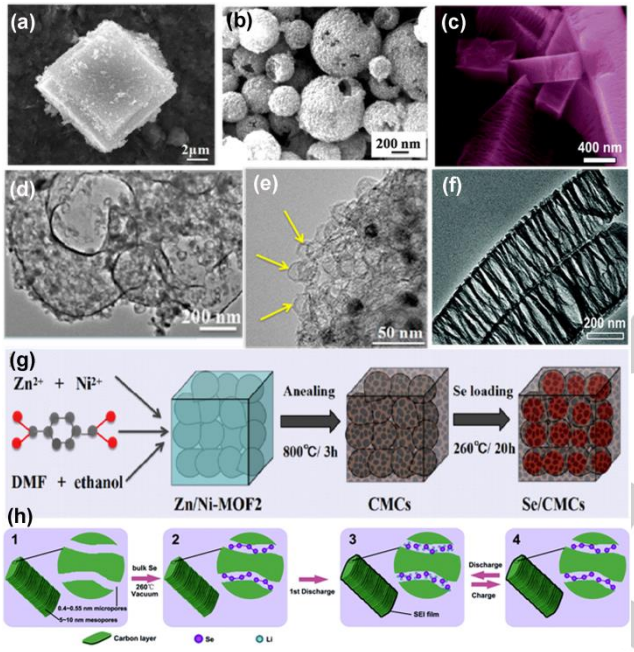

Figure 13. (a-c) The SEM images of three SBU structures and their corresponding TEM images (d-f). (g) Illustration of the synthesis route for the Se/CMCs. (h) Schematic discharge-charge mechanism of the NCS/Se-50 composite cathode. [Reprinted with permission from Ref. [140,141]. Copyright 2016, American Chemical Society. Copyright 2017, Elsevier. Reproduced from Ref. [142] with permission from The Royal Society of Chemistry.].

In summary, MOFs derived porous carbon can provide high specific surface area and high electrical conductivity for sulfur or selenium cathode. The physical and chemical absorptions in Li-S/Li-Se batteries can enhance the cycling stability of batteries. Heteroatoms doping (such as N, B, P) can further improve the electrical conductivity and the structural stability of the materials. The above-mentioned methods are all useful for modifying the electrochemical performances of Li-S/Li-Se batteries.

4. MOFs-derived cathode materials for Li-O_2 batteries

Li-O_2 (Li-air) batteries show higher energy density (3458 Wh kg^{-1}) compared to Li-S/Li-Se batteries,[145,146] and therefore they can act as efficient energy storage systems to meet the needs of electric and hybrid vehicles' development. Actually, Li-O_2 batteries are composed of metal lithium anode and O_2 cathode. It is widely accepted that beside the cathode reaction in Eq. 8, there are two inevitable side reactions such as disproportionation (Eq. 9) and electro-reduction (Eq. 10).[147] The insoluble and insulating Li_2O_2 is deposited on the oxygen cathode, causing the pores to be clogged and the catalytic sites to be blocked,[148] and hence leading to over potential of electrodes in Li-O_2 batteries. Another significant challenge for Li-O_2 batteries is that the kinetics of oxygen evolution reaction (OER) and oxygen reduction reaction (ORR) is sluggish, and this directly limits the electrochemical performances of Li-O_2 batteries.[149,150] Li-O_2 batteries are generally operated in pure oxygen to increase the concentration of O_2 and to avoid the interference caused by H_2O and CO_2.[151,152] This limitation also restricts the application of Li-O_2 batteries.

$$O_2 + e^- + Li^+ = LiO_2 \quad (8)$$

$$LiO_2 + LiO_2 = Li_2O_2 + O_2 \quad (9)$$

$$LiO_2 + e^- + Li^+ = Li_2O_2 \quad (10)$$

Metal-organic frameworks (MOFs) are known for their controlled pore structures, huge specific surface area and active metal sites. Therefore, MOFs are also excellent catalytic materials, which improve the utilization of oxygen and modify the electrochemical performances of Li-O_2 batteries. In this section, we review the progress in developing the MOFs based cathode materials for Li-O_2 batteries, which has been made since 2012. In detail, we divide MOFs derived cathode materials into three categories considering their functions: oxygen reservoirs, catalysts and MOFs membranes for gas separation.

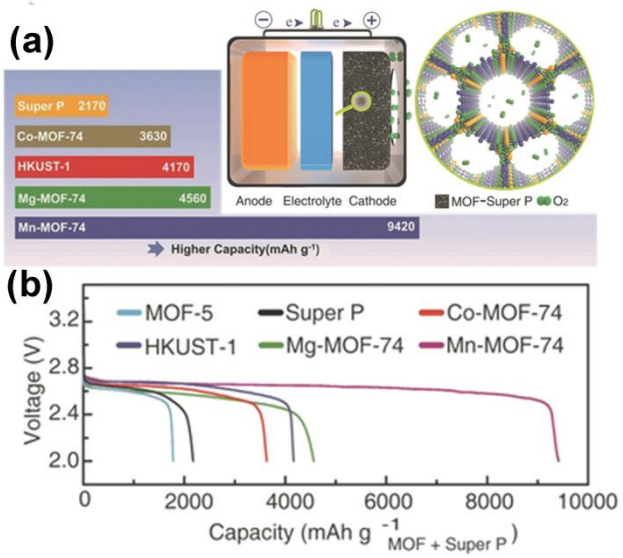

Figure 14. (a) Schematic illustration of a Li-O_2 cell using MOF-Super P composite as the O_2 electrode. Oxygen molecules relative sizes reduced for clarity. (b) Discharge profiles of the Li-O_2 cells using MOF-Super P composites or Super P only under O_2 atmosphere with a current of 50 mA g^{-1} at room temperature. [Reprinted with permission from Ref. [153], Copyright 2014, Wiley.].

Employing MOFs as oxygen reservoirs for Li-O_2 batteries was inspired by the development of sulfur/MOF cathodes in Li-S batteries. Li et al.[153] explored the feasibility of different MOFs as O_2 reservoirs for cathodes and found that MOFs could increase the concentration of O_2 in the micropores by up to 18 times under ambient pressure at 273 K. Oxygen is stored in the pore structure of the MOFs (Figure 14a). The charging-dishcharging tests demonstrated that different MOF cathodes had different electrical properties. For example, Mn-MOF-74/Super P composite delivered a primary discharge capacity of 9420 mA h g^{-1} under 1 atm of O_2 at room temperature. However, the discharge capacity of MOF-5/Super P was less than 2000 mA h g^{-1} under the same test condition (Figure 14b). Li et al. ascribed this excellent capacity to both the increase of O_2 concentration in porous structure and the enhancement of reaction efficiency caused by open metal sites.

From our point of view, the reaction efficiency improvement in the Mn-MOF-74/Super P composite cathode is the manifestation of catalytic effect of metal's active sites. Many efforts have been made by scientists to improve ORR activities by utilizing MOFs as catalysts for Li-O_2 battery cathodes.[154,155] Wu et al. synthesized graphene/graphene-tube-rich N-Fe-MOF catalysts as cathode of Li-O_2 batteries.[156] The catalysis of Fe-MOF raised the discharge capacity to 5300 mA h g^{-1}, which is much higher than those of N-doped CNTs (866 mA h g^{-1}) and N-doped graphene (3700 mA h g^{-1}). The aim of synthesizing bimetal MOFs is to introduce more defects into MOFs, and thereby significantly to improve the catalytic activity of MOFs.[157,158] By using this strategy, Chen et al. obtained the porous cobalt-manganese oxide (Co-Mn-O) nanocubes with high electrocatalytic activity.[159] Both bimetal structure design and morphology tailoring can decrease the cathode overpotential and improve the electrochemical performances of cathodes. The porous Co-Mn-O nanocube sample delivered an excellent cycle stability until 100 cycles at 0.16 mA cm^{-2}. Wang et al.[160] prepared the hierarchical Zn/Ni-MOF-2 nanosheet-assembled hollow nanocubes in order to improve the catalytic performances of cathode in Li-O_2 batteries. The unique nanostructure can be created by a solvothermal route, and the crystal structure transformation can be controlled by varying the synthetic condition. By extrusion-based 3D printing of Co-MOF-based precursors, Wang et al.[161] synthesized hierarchical porous carbon frameworks with Co nanocatalysts. Owing to the synergistic effect between hierarchically pores and Co nanoparticle catalyst, a high practical specific energy (798 Wh kg^{-1}_{cell}) was achieved in Li-O_2 batteries. This strategy provides more possibilities for structural design of Li-O_2 batteries. Zhou et al.[162] designed a MOF($Cu_3(BTC)_2$)-based separator with a narrow pore size window, which acted as a redox mediating molecular sieve, to restrain the electron shuttling in Li-O_2 batteries. Through this strategy, the obtained Li-O_2 battery revealed an excellent cycling performance (5000 mA h g^{-1} after 100 cycles) at the high current density of 1000 mA g^{-1}.

There are three challenges that block the applications of Li-O_2 batteries in atmospheric air. First, the moisture from air leads to oxidation of lithium and further causes battery safety problems. Second, CO_2 from air causes side reactions producing Li_2CO_3 and hence, poor electrochemical performances. Third, the concentration of O_2 in air is too low to ensure the normal operation of Li-O_2 batteries at high current density. O_2-selective membrane, through which except oxygen other types of gases cannot pass, is a promising material enabling Li-O_2 batteries to be used in air. Therefore, MOF, which is a classical porous material with tunable pore size, is explored as an O_2 selective membrane for Li-O_2 batteries.[163] Lu et al.[164] fabricated an effective O_2 selective membrane by incorporating polydopamine-coated MOF crystals of CAU-1-NH_2 into a polymethylmethacrylate (PMMA) matrix for Li-O_2 batteries working in air. They used abundant functional groups to absorb CO_2 and used the hydrophobic behavior of the PMMA to prevent H_2O from entering the Li-O_2 batteries.

Table 1. Electrochemical performances of various cathode materials

Compounds	Battery types	Operating voltage window (V)	Low-rate capability (mA h g^{-1})	High-rate capability (mA h g^{-1})	Ref.
$K_{2.5}[(VO)_2(HPO_4)_{1.5}(PO_4)_{0.5}(C_2O_4)]$	LIBs	2.5-4.6	68 after 60 cycles at 0.4 C	40 after 60 cycles at 2 C	58
$rGO/K_2[(VO)_2(HPO_4)_2(C_2O_4)]$	LIBs	2.5-4.5	100 after 20 cycles at 0.5 C	57 (±3) at 4 C	60
$Li_2(VO)_2(HPO_4)_2(C_2O_4)\cdot 6H_2O$	LIBs	2.5-4.5	80 after 25 cycles at 0.1 C	47 after 20 cycles at 500 mA g^{-1}	61
$Li_3V_2(PO_4)_3/C$	LIBs	2.5-4.3	132 after 30 cycles at 0.1 C	97 at 10 C, 56(±3) at 20 C	62
$Li_3V_2(PO_4)_3$/phosph-orus-doped C	LIBs	3.0-4.3	138 at 0.1 C	58 after 1100 cycles at 10 C	63
$KFe_2(CN)_6$	SIBs	2.0-4.0	100 at 0.05 C	-	32
$KMnFe(CN)_6$			~70 at 0.05 C	-	
$KCoFe(CN)_6$			~55 at 0.05 C	-	
$KNiFe(CN)_6$			~50 at 0.05 C	-	
$KCuFe(CN)_6$			~55 at 0.05 C	-	
$KZnFe(CN)_6$			~33 at 0.05 C	-	
$FeFe(CN)_6$	SIBs	2.0-4.0	120 at 0.5 C	98 at 10 C, 67 after 500 cycles at 20 C	68
$KCuFe(CN)_6$	K-ion battery	0.6-1.4	59.14 at 0.83 C	40.1 after 100 cycles at 83 C	69
$K_{0.36}Ni_{1.2}Fe(CN)_6\cdot 3.6H_2O$	SIBs	0.3-0.9	59 at 0.83 C	39 at 41.7 C	70
$Na_{1.72}MnFe(CN)_6$	SIBs	2.0-4.2	121 after 30 cycles at 0.05 C	45 at 40 C	71
$Na_{1.70}FeFe(CN)_6$	SIBs	2.0-4.2	120.7 at 200 mA g^{-1}	73.6 at 1200 mA g^{-1}	72
$Na_{1.56}FeFe(CN)_6\cdot 3.1H_2O$	SIBs	2.0-4.0	103 at 20 mA g^{-1}	100 after 400 cycles at 20 mA g^{-1}	73
$Na_{3.27}Fe_{0.35}[Fe(CN)_6]\cdot 0.85H_2O$	SIBs	2.0-4.5	103 at 0.22 C	70 after 100 cycles 0.89 C	74
$Na_{0.61}Fe[Fe(CN)_6]_{0.94}$	SIBs	2.0-4.2	170 after 150 cycles at 25 mA g^{-1}	110 at 150 mA g^{-1}, 70 at 600 mA g^{-1}	75
$R\text{-}Na_{1.92}Fe[Fe(CN)_6]$	SIBs	2.0-4.0	160 at 10 mA g^{-1}	120 after 1000 cycles at 300 mA g^{-1}	76
$Na_2Mn_{0.15}Co_{0.15}Ni_{0.1}Fe_{0.6}Fe(CN)_6$	SIBs	2.0-4.0	117 at 0.1 C	87.4 after 1500 cycles at 1 C	77

Compounds	Battery types	Operating voltage window (V)	Low-rate capability (mA h g^{-1})	High-rate capability (mA h g^{-1})	Ref.
RGO/$Na_{0.81}Fe[Fe(CN)_6]_{0.94}$*□$_{0.21}$ (□=$Fe(CN)_6$ vacancy)	SIBs	2.0-4.0	163 at 30 mA g^{-1}	137.6 after 500 cycles at 200 mA g^{-1}	79
$Na_{0.647}Fe[Fe(CN)_6]_{0.93}$*□$_{0.03}$·$2.6H_2O$ /C	SIBs	2.0-4.0	~133 at 0.5 C	77.5 at 90 C, 90 after 2000 cycles at 20 C	64
$KNiFe(CN)_6$	SIBs	2.5-3.8	65 at 10 mA g^{-1}	52 at 500 mA g^{-1}	80
$FeFe(CN)_6$	aqueous SIBs	-0.2-1.1	125 at 1 C	84.7 after 500 cycles at 20 C	81
$Ni_2Fe(CN)_6$||$Ni0._{67}Fe_{0.33}Se_2$	SIBs full cell	0.5-3.0	354.6 at 1.0 A g^{-1}	302 after 30 cycles at 1.0 A g^{-1}	82
$Na_2MnFe(CN)_6$||$NaTi_2(PO_4)_3$	aqueous SIBs full cell	0.5-1.5	57 at 0.1 A g^{-1}	32 at 0.2 A g^{-1}	85
$Na_2Mn[Fe(CN)_6]$||$KMn[Cr(CN)_6]$	aqueous SIBs full cell	0.5-2.5	-	~22 after 100 cycles at 30 C	86
MIL-53(Fe)·H_2O	LIBs	1.5-3.5	~70 after 50 cycles at 0.025 C	-	88
MIL-53(Fe)	LIBs	1.8-3.5	93 at 0.1 C	-	89
MIL-68(Fe)	LIBs	1.5-3.5	40 at 0.02 C	-	90
MIL-136(Ni)	LIBs	2.0-4.3	-	20 at 10 C	92
MIL-47(V)	LIBs	1.6-3.5	118 at 0.1 C	40 at 10 C	93
MIL-132(K)	LIBs	2.3-3.8	-	~40 at 10 C	94
MIL-88B derived FeOF-H_2SiF_6/graphitic carbon layers	LIBs	1.2-4.0	455 after 30 cycles at 20 mA g^{-1}	338 after 100 cycles at 100 mA g^{-1}	96
MIL-53(Fe) derived 3D porous carbon/FeF_3·$0.33H_2O$	LIBs	1.7-4.5	133 after 300 cycles at 5 C	86 at 20 C	97
UiO-66 derived ZrO_2 coated $LiCoO_2$	LIBs	3.0-4.5	-	134 after 100 cycles at 13 C	99
UiO-66 derived ZrO_2 coated $Li_{1.2}Mn_{0.54}Co_{0.13}Ni_{0.13}O_2$	LIBs	2.0-4.8	279 at 0.1 C	110 at 5 C	100
MIL-101(V) derived carbon coated $Li_3V_2(PO_4)_3$	LIBs	3.0-4.8	113.1 after 1000 cycles at 0.5 C	105.8 after 1000 cycles at 1 C	101
MIL-100(Cr)/Sulfur	Li-S battery	1.0-3.0	1580 at 0.1 C	-	118
Sulfur@MOFs(HKUST-1)/CNT	Li-S battery	1.0-3.0	1263 at 0.2 C	880 at 2 C, 449 at 10 C	119
Sulfur/ZIF-8	Li-S battery	1.8-2.8	1055 at 0.1 C	710 at 1C	120
Mn-based MOF/Sulfur	Li-S battery	1.7-2.8	990 after 200 cycles at 0.2 C	743 after 200 cycles at 1 C	122
Sulfur@Cu-MOF (Cu-TDPAT)	Li-S battery	1.8-2.8	~1000 at 0.1 C	745 after 500 cycles at 1 C	123
Graphene-wrapped MIL-101(Cr)/sulfur	Li-S battery	1.0-3.0	1190 at 0.1 C	809 after 134 cycles at 0.8 C	124
Thermal exfoliation of MOF into multilayer graphene stacks/Sulfur	Li-S battery	1.7-2.7	-	~700 after 100 cycles at 1 C	125
Sulfure/ZIF-8@Carbon nanotubes	Li-S battery	1.7-2.7	1380 at 0.1 C	750 after 500 cycles at 1 C	126
MOF-5-derived HPC/sulfur	Li-S battery	1.5-3.0	919.4 at 400 mA g^{-1}	-	129
MOF-5-derived HPC/sulfur	Li-S battery	1.0-3.0	1177 at 0.1 C	730 after 50 cycles at 0.5 C	130
MOF(Al)-derived HPC/sulfur	Li-S battery	1.5-2.8	1200 at 0.1 C	763 after 200 cycles at 2 C	131
MOF-derived porous carbon/graphene@sulfur	Li-S battery	1.8-2.8	1372 at 0.1 C	608 after 300 cycles at 1 C	132
Sulfur/Nitrogen-doped carbon (derived from ZIF-8)	Li-S battery	1.0-3.0	936 after 100 cycles at 335 mA g^{-1}	632 at 5 A g^{-1}	133
MOF-derived CMCs/Se	Li-Se battery	1.0-3.0	425 after 100 cycles at 0.2 C	218.1 after 50 cycles at 5 C	140
MOF-derived hollow HPC/Se	Li-Se battery	1.0-3.0	588.2 at 0.5 C	200 after 1000 cycles at 1 C	141
MOF-derived HPC/Se	Li-Se battery	1.0-3.0	443.2 after 200 cycles at 0.5 C	286.6 at 5 C	142
ZIF derived core-shell HPC/Se	Li-Se battery	1.0-3.0	555 after 150 cycles at 0.2 C	432 after 200 cycles at 1 C	143
Zn-glutamate MOF derived HPC/Se	Li-Se battery	1.0-3.0	612 after 200 cycles at 0.2 C	~420 after 500 cycles at 0.5 C	144
MOF-5	Li-O_2 battery	2.0-4.5	<2000 at 50 mA g^{-1} for the first cycle	-	153
Co-MOF-74			3630 at 50 mA g^{-1} for the first cycle	-	
HKUST-1			4170 at 50 mA g^{-1} for the first cycle	-	
Mg-MOF-74			4560 at 50 mA g^{-1} for the first cycle	-	
Mn-MOF-74			9420 at 50 mA g^{-1} for the first cycle	-	
graphene/graphee-tube derived from MOF(Fe)	Li-O_2 battery	2.1-3.5	5300 at 400 mA g^{-1}	-	156
MOF derived ZnO/$ZnFe_2O_4$/C	Li-O_2 battery	2.4-4.3	11000 at 300 for mA g^{-1} the first cycle	5000 after 15 cycles at 300 mA g^{-1}	158
Porous Cobalt Manganese oxide nanocubes derived from MOF	Li-O_2 battery	2.0-4.5	7653 at 0.04 mA cm^{-2}	500 after 100 cycles at 0.16 mA cm^{-2}	159
Co-MOF derived C/Co	Li-O_2 battery	2.0-3.2	1124 at 0.05 mA cm^{-2}	525 at 0.8 mA cm^{-2}	161
Li_2S/Cu-MOF	Li-S battery	1.5-2.6	1051.3 after 300 cycles at 200 mA g^{-1}	-	165
MOF-derived N-Co_3O_4@N-C/RGO	Li-S battery	1.7-2.7	945 after 300 cycles at 0.2 C	611 after 1000 cycles at 2 C	166
Ba and Ti doped $LiCoO_2$	LIBs	3.0-4.6	169.9 after 200 cycles at 0.2 C	~100 at 5 C	167
$Li(Li_{0.05}Ni_{0.7-x}Mn_{0.25}Co_x)O_2$	LIBs	2.8-4.5	167 at 0.5 C	120 after 20 cycles at 2 C	168
$Li_3V_2(PO_4)_3$/hard carbon	LIBs	3.0-4.3	143 at 0.1 C	92 after 1000 cycles at 10 C	169

Compounds	Battery types	Operating voltage window (V)	Low-rate capability (mA h g^{-1})	High-rate capability (mA h g^{-1})	Ref.
$Li_2NaV_2(PO_4)_3$/hard carbon	LIBs	3.0-4.3	137.2 at 0.1 C	76 after 300 cycles at 10 C	170
$Na_3V_2(PO_4)_3$	SIBs	2.3-3.9	116 at 0.1 C	63 at 30 C	171

5. Summary and Outlook

In order to directly compare the electrochemical performances of the batteries with different MOF-derived cathode materials, the reported performance-indicating values are shown in table 1. To give a better overview of the MOF-related cathode materials, some additional crucial examples, which have not been described in detail in the present article, along with some currently used ones, are also listed in table 1.[165-171]

In this article, we have reviewed the recent advances in developing the MOF-based composites as cathodes used in LIBs, SIBs, Li-S/Se batteries and Li-O_2 batteries. It is generally accepted that the fascinating features of MOFs, such as huge specific surface area, high porosity, active metal sites, controllable morphology and adjustable pore structures, can be used to modify and greatly enhance the electrochemical performances of the cathode materials. These features allow MOFs not only to adsorb more electrolytes and to provide more reaction sites for batteries, but also to increase the storage efficiency of S/O_2. The adjustability of pore structure and size makes the optimization of MOFs possible when they function as separating membrane for Li-O_2 batteries. Owing to the high catalytic activity of metal sites, MOFs can be used as an important component of cathodes to enhance the Li-O_2 battery performances.

Nonetheless, several major challenges remain for the practical applications of MOFs based cathode materials as follows. (1) The yield of MOFs is too low to satisfy the demands for the mass fabrication of cathodes. (2) The structural stability of MOFs should be further improved to increase the discharging/charging cycling stability. Simultaneously, the electron conductivity in the MOFs based host materials should be increased by tuning the chemistry and structure of the ligands. (3) The catalytic performance of MOFs need to be further enhanced to raise the reaction efficiency in Li-O_2 batteries. (4) The structure and morphology of MOFs should be further optimized to improve the high-rate performance for all types of batteries described in this article. Li-O_2 batteries have the worst high-rate performance, followed by Li-S/Se batteries, SIBs, and LIBs. The potential for MOF structure and morphology to be improved concerning the high-rate performance of batteries should follow this sequence: Li-O_2 batteries>Li-S/Se batteries>SIBs>LIBs. From our perspective, the design of the second building units (Figure 13g) might be an effective strategy to acquire ideal structures for cathode materials. In addition, the mechanism of the impact of MOF structure on the electrochemical properties should be further clarified.

On one hand, it is a promising way to use MOF-based materials as a main component of cathodes in order to improve the battery performances. On the other hand, it is still a big challenge to commercialize the MOF-based cathodes due to the limitation of the current technology for mass production. There are different approaches for tailoring the properties of the MOF-based cathodes. For instance, MOFs contain transition metal sites, where redox reactions occur, which are the prerequisite for enhancing the electrochemical functions of cathode materials. The transition metals in MOFs are exchangeable, which is thus advantageous for optimizing battery performances. Furthermore, the effort should be made to maintain the structure of MOFs in cathode during cathode fabrication and long cycling process, thereby benefiting the lithium ion storage and transfer.

Acknowledgements

This work was supported by National Natural Science Foundation of China (Nos: 51772223, 51372180, 51802236), and Corning Incorporated, USA.

Keywords: metal-organic frameworks • cathodes • superior electrochemical performances • batteries

Notes and references

[1] Q. Xu, J. Y. Li, J. K. Sun, Y. X. Yin, L. J. Wan, Y. G. Guo, *Adv. Energy Mater.*, **2017**, *7*, 1601481.
[2] D. J. Lee, S. H. Yu, H. S. Lee, A. Jin, J. Lee, J. E. Lee, Y. E. Sung, T. Hyeon, *J. Mater. Chem. A*, **2017**, *5*, 8744-8751.
[3] P. Pietsch, V. Wood, *annu. Rev. Mater. Res.*, **2017**, *47*, 12.11-12.29.
[4] S. Wilke, B. Schweitzer, S. Khateeb, S. Al-Hallaj, *J. Power Sources.*, **2017**, *340*, 51-59.
[5] K. K. Lee, K. Park, H. Lee, Y. Noh, D. Kossowska, K. Kwak, M. Cho, *Nat. Commun.*, **2017**, *8*, 14658.
[6] L. Liang, X. Sun, J. Zhang, J. Sun, L. Hou, Y. Liu, C. Yuan, *Mater. Horiz.*, **2019**, DOI: 10.1039/c8mh01593g.
[7] C. H. Wang, Y. V. Kaneti, Y. Bando, J. J. Lin, C. Liu, J. S. Li, Y. Yamauchi, *Mater. Horiz.*, **2018**, *5*, 394-407.
[8] L. M. Suo, O. Borodin, Y. S. Wang, X. H. Rong, W. Sun, X. L. Fan, S. Y. Xu, M. A. Schroeder, A. V. Cresce, F. Wang, C. Y. Yang, Y. S. Hu, K. Xu, C. S. Wang, *Adv. Energy Mater.*, **2017**, *7*, 1701189.
[9] W. H. Li, S. H. Hu, X. Y. Luo, Z. L. Li, X. Z. Sun, M. S. Li, F. F. Liu, Y. Yu, *Adv. Mater.*, **2017**, *29*, 160820.
[10] T. Y. Ma, G. L. Xu, X. Q. Zeng, Y. Li, Y. Ren, C. J. Sun, S. M. Heald, J. Jorne, K. Amine, Z. Chen, *J. Power Sources.*, **2017**, *341*, 114-121.
[11] G. X. Li, J. H. Sun, W. P. Hou, S. D. Jiang, Y. Huang, J. X. Geng, *Nat. Commun.*, **2016**, *7*, 10601.
[12] Z. Ma, X. X. Yuan, L. Li, Z. F. Ma, D. P. Wilkinson, L. Zhang, J. J. Zhang, *Energy. Environ. Sci.*, **2015**, *8*, 2144-2198.
[13] K. Han, Z. Liu, J. M. Shen, Y. Y. Lin, F. Dai, H Q. Ye, *Adv. Funct Mater.*, **2015**, *25*, 455-463.
[14] M. Winter, B. Barnett, K. Xu, *Chem. Rev.*, **2018**, *118*, 11433-11456.
[15] A. Bauer, J. Song, S. Vail, W. Pan, J. Barker, Y. H. Lu, *Adv. Energy Mater.*, **2018**, *8*, 1702869.
[16] X. H. Yao, Z. X. Zhu, Q. Li, X. P. Wang, X. M. Xu, J. S. Meng, W. H. Ren, X. H. Zhang, Y. H. Huang, L. Q. Mai, *ACS Appl. Mater. Interfaces*, **2018**, *10*, 10022-10028.
[17] Y. J. Chen, Y. L. Xu, X. F. Sun, C. Wang, *J. Power Sources*, **2018**, *375*, 82-92.
[18] H. C. Gao, I. D. Seymour, S. Xin, L. G. Xue, G. Henkelman, J. B. Goodenough, *J. Am. Chem. Soc.*, **2018**, *140*, 18192-18199.
[19] J. M. Fan, G. S. Li, B. Y. Li, D. Zhang, D. D. Chen, L. P. Li, *ACS. Appl. Mater. Interfaces*, **2019**, *11*, 19950-19958.
[20] X. N. Li, J. W. Liang, X. Li, C. H. Wang, J. Luo, R. Y. Li, X. L. Sun, *Energy Environ. Sci.*, **2018**, *11*, 2828-2832.

[21] W. L. Li, J. Qian, T. Zhao, Y. S. Ye, Y. Xing, Y. X. Huang, L. Wei, N. X. Zhang, N. Chen, L. Li, F. Wu, R. J. Chen, *Adv. Sci.*, **2019**, 1802362.
[22] W. K. Ye, W. Y. Li, K. Wang, W. H. Yin, W. W. Chai, Y. Qu, Y. C. Rui, B. H. J. Tang, *J. Phys. Chem. C*, **2019**, *123*, 2048-2055.
[23] Y. B. He, Z. Chang, S. C. Wu, Y. Qiao, S. Y. Bai, K. Z. Jiang, P. He, H. S. Zhou, *Adv. Energy Mater.,* **2018**, *8*, 1802130.
[24] D. F. Wu, Z. Y. Guo, X. B. Yin, Q. Q. Pang, B. B. Tu, L. J. Zhang, Y. G. Wang, Q. W. Li, *Adv. Mater.*, **2014**, *26*, 3258-3262.
[25] W, J. Kwak, H. Kim, H. G. Jung, D. Aurbach, Y. K. Sun, *J. Electrochem. Soc.*, **2018**, *165*, A2274-A2293.
[26] A. Dai, Q. D. Li, T. C. Liu, K. Amine, J. Lu, *Adv. Mater.*, **2018**, *31*, 1805602.
[27] O. M. Yaghi, H. L. Li, *J. Am. Chem. Soc.*, **1995**, *117*, 10401-10402.
[28] G. Y. Xu, P. Nie, H. Dou, B. Ding, L. Y. Li, X. G. Zhang, *Mater. Today*, **2017**, *20*, 191-209.
[29] L. Wang, Y. Z. Han, X. Feng, J. W. Zhou, P. F. Qi, B. Wang, *Coordin. Chem. Rev.*, **2016**, *307*, 361-381.
[30] H. Furukawa, K. E. Cordova, M. O'Keeffe, O. M. Yaghi, *Science*, **2013**, *341*, 1230444.
[31] P. G. Yot, Z. Boudene, J. Macia, D. Granier, L. Vanduyfhuys, T. Verstraelen, V. V. Speybroeck, T. Devic, C. Serre, G. Férey, N. Stock, G. Maurin, *Chem. Commun.*, **2014**, *50*, 9462-9464.
[32] Y. H. Lu, L. Wang, J. G. Cheng, J. B. Goodenough, *Chem. Commun.*, **2012**, *48*, 6544-6546.
[33] D. P. Cai, H. B. Zhan, T. H. Wang, *Mater. Lett.*, **2017**, *197*, 241-244.
[34] Q. He, J. S. Liu, Z. H. Li, Q. Li, L. Xu, B. X. Zhang, J. S. Meng, Y. Z. Wu, L. Q. Mai, *Small*, **2017**, *13*, 1701504.
[35] K. Shen, L. Chen, J. L. Long, W. Zhong, Y. W. Li, *ACS Catal.*, **2015**, *5*, 5264-5271.
[36] F. C. Zheng, Y. Yang, Q. W. Chen, *Nat. Commun.*, **2014**, *5*, 5261.
[37] D. J. Tranchemontagne, J. R. Hunt, O. M. Yaghi, *Tetrahedron*, **2008**, *64*, 8553-8557.
[38] M. R. DeStefano, T. Islamoglu, S. J. Garibay, J. T. Hupp, O. K. Farha, *Chem. Mater.*, **2017**, *29*, 1357-1361.
[39] X. F. Lu, L. F. Gu, J. W. Wang, J. X. Wu, P. Q. Liao, G. R. Li, *Adv. Mater.*, **2017**, *29*, 1604437.
[40] J. Aguilera-Sigalat, D. Bradshaw, *Coordin. Chem. Rev.*, **2016**, *307*, 267-291.
[41] N. Stock, S. Biswas, *Chem. Rev.*, **2012**, *112*, 933-969.
[42] X. Liu, W. T. Fu, E. Bouwman, *Chem. Commun.*, **2016**, *52*, 6926-6929.
[43] H. S. Lu, L. L. Bai, W. W. Xiong, P. Z. Li, J. F. Ding, G. D. Zhang, T. Wu, Y. L. Zhao, J. M. Lee, Y. H. Yang, B. Y. Geng, Q. C. Zhang, *Inorg Chem.*, **2014**, *53*, 8529-8537.
[44] L. G. Qiu, Z. Q. Li, Y. Wu, W. Wang, T. Xu, X. Jiang, *Chem. Commun.*, **2008**, *0*, 3642-3644.
[45] Z. Ni, R. I. Masel, *J. Am. Chem. Soc.*, **2006**, *128*, 12394-12395.
[46] H. Bux, F. Y. Liang, Y. S. Li, J. Cravillon, M. Wiebcke, J. Caro, *J. Am. Chem. Soc.*, **2009**, *131*, 16000-16001.
[47] X. H. Cao, C. L. Tan, M. Sindoro, H. Zhang, *Chem. Soc. Rev.*, **2017**, *46*, 2660-2677.
[48] Y. Zhao, Z. X. Song, X. Li, Q. Sun, N. C. Cheng, S. Lawes, X. L. Sun, *Energy Storage Materials*, **2016**, *2*, 35-62.
[49] W. Xia, A. Mahmood, R. Zou, Q. Xu, *Energy Environ. Sci.*, **2015**, *8*, 1837-1866.
[50] A. E. Baumann, D. A. Burns, B. Q. Liu, V. S. Thoi, *Commun Chem.*, **2019**, Doi:10.1038/s42004-019-0184-6.
[51] Y. Nishi, *J. Power Soureces.*, **2001**, *100*, 101-106.
[52] B. Zhao, R. Ran, M. Liu, Z. Shao, *Mat. Sci. Eng. R.*, **2015**, *98*, 1-71.
[53] P. Nugent, Y. Belmabkhout, S. D. Burd, A. J. Cairns, R. Luebke, K. Forrest, T. Pham, S. Q. Ma, B. Space, L. Wojtas, M. Eddaoudi, M. J. Zaworotko, *Nature*, **2013**, *495*, 80-84.
[54] J. A. Mason, J. Oktawiec, M. K. Taylor, M. R. Hudson, J. Rodriguez, J. E. Bachman, M. I. Gonzalez, A. Cervellino, A. Guagliardi, C. M. Brown, P. L. Llewellyn, N. Masciocchi, J. R. Long, *Nature*, **2015**, *527*, 357-361.
[55] Z. Chang, D. H. Yang, J. Xu, T. L. Hu, X. H. Bu, *Adv. Mater.*, **2015**, *27*, 5432-5441.
[56] G. K. H. Shimizu, J. M. Taylor, S. Kim, *Science*, **2013**, *341*, 354-355.
[57] C. B. He, D. M. Liu, W. B. Lin, *Chem. Rev.*, **2015**, *115*, 11079-11108.
[58] M. Nagarathinam, K. Saravanan, E. J. H. Phua, M. V. Reddy, B. V. R. Chowdari, J. J. Vittal, *Angew. Chem. Int. Ed.*, **2012**, *51*, 5866-5870.
[59] T. Wei, M. Zhang, P. Wu, Y. J. Tang, S. L. Li, F. C. Shen, X. L. Wang, X. P. Zhou, Y. Q. Lan, *Nano Energy*, **2017**, *34*, 205-214.
[60] A. S. Hameed, M. V. Reddy, M. Nagarathinam, T. Runčevski, R. E. Dinnebier, S. Adams, B. V. R. Chowdari, J. J. Vittal, *Sci. Rep.*, **2015**, *5*, 16270.
[61] A. S. Hameed, M. Nagarathinam, M. Schreyer, M. V. Reddy, B. V. R. Chowdari, J. J. Vittal, *J. Mater. Chem. A.*, **2013**, *1*, 5721-5726.
[62] A. S. Hameed, M. V. Reddy, B. V. R. Chowdari, J. J. Vittal, *Electrochim. Acta.*, **2014**, *128*, 184-191.
[63] Z. Y. Wang, W. He, X. D. Zhang, Y. Z. Yue, J. H. Liu, C. J. Zhang, L.-Y. Fang, *J. Power Sources.*, **2017**, *366*, 9-17.
[64] Y. Z. Jiang, S. L. Yu, B. Q. Wang, Y. Li, W. P. Sun, Y. H. Lu, M. Yan, B. Song, S.-X. Dou, *Adv. Funct. Mater.*, **2016**, *26*, 5315-5321.
[65] Y. Ding, Y. Zhao, Y. T. Li, J. B. goodenough, G. H. Yu, *Energy Environ. Sci.*, **2017**, *10*, 491-497.
[66] L. Wu, T. Moteki, A. A. Gokhale, D. W. Flaherty, F. D. Toste, *Chem*, **2016**, *1*, 32-58.
[67] S. H. Shin, S. H. Yun, S. H. Moon, *RSC Adv.*, **2013**, *3*, 9095-9116.
[68] X. Y. Wu, W. W. Deng, J. F. Qian, Y. L. Cao, X. P. Ai, H. X. Yang, *J. Mater. Chem. A*, **2013**, *1*, 10130-10134.
[69] C. D. Wessells, R. A. Huggins, Y. Cui, *Nat. Commun.*, **2011**, *2*, 550.
[70] C. D. Wessells, S. V. Peddada, R. A. Huggins, Y. Cui, *Nano lett.*, **2011**, *11*, 5421-5425.
[71] L. Wang, Y. H. Lu, J. Liu, M. W. Xu, J. G. Cheng, D. W. Zhang, J. B. Goodenough, *Angew. Chem. Int. Ed.*, **2013**, *52*, 1964-1967.
[72] Y. Liu, Y. Qiao, W. X. Zhang, Z. Li, X. Ji, L. Miao, L. X. Yuan, X. L. Hu, Y. H. Huang, *Nano Energy*, **2015**, *12*, 386-393.
[73] W. J. Li, S. L. Chou, J. Z. Wang, Y. M. Kang, J. L. Wang, Y. Liu, Q. F. Gu, H. K. Liu, S. X. Dou, *Chem. Mater.*, **2015**, *27*, 1997-2003.
[74] L. Li, P. Nie, Y. B. Chen, J. Wang, *J. Mater. Chem. A*, **2019**, *7*, 12134-12144.
[75] Y. You, X. L. Wu, Y. X. Yin, Y. G. Guo, *Energy Environ. Sci.*, **2014**, *7*, 1643-1647.
[76] L. Wang, J. Song, R. M. Qiao, L. A. Wray, M. A. Hossain, Y. D. Chuang, W. L. Yang, Y. H. Lu, D. Evans, J. J. Lee, S. Vail, X. Zhao, M. Nishijima, S. Kakimoto, J. B. Goodenough, *J. Am. Chem. Soc.*, **2015**, *137*, 2548-2554.
[77] B. X. Xie, P. J. Zuo, L. G. Wang, J. J. Wang, H. Huo, M. X. He, J. Shu, H. F. Li, S. F. Lou, G. P. Yin, *Nano Energy*, **2019**, *61*, 201-210.
[78] X. Y. Guo, Z. B. Wang, Z. Deng, X. G. Li, B. Wang, X. Chen, S. P. Ong, *Chem. Mater.*, **2019**, Doi: 10.1021/acs.chemmater.9b02269.
[79] D. Y. Yang, J. Xu, X. Z. Liao, H. Wang, Y. S. He, Z. F. Ma, *Chem. Commun.*, **2015**, *51*, 8181-8184.
[80] Y. F. Yue, A. J. Binder, B. K. Guo, Z. Y. Zhang, Z. A. Qiao, C. C. Tian, S. Dai, *Angew. Chem. Int. Ed.*, **2014**, *53*, 3134-3137.
[81] X. Y. Wu, Y. Luo, M. Y. Sun, J. F. Qian, Y. L. Cao, X. P. Ai, H. X. Yang, *Nano Energy*, **2015**, *13*, 117-123.
[82] P. Ge, S. J. Li, H. L. Shuai, W. Xu, Y. Tian, L. Yang, G. Q. Zou, H. S. Hou, X. B. Ji, *Adv. Mater*. **2018**, *31*, 1806092.
[83] J. W. Nai, X. W. Lou, *Adv. Mater*. **2018**, 1706825.
[84] J. F. Qian, C. Wu, Y. L. Cao, Z. F. Ma, Y. H. Huang, X. P. Ai, H. X. Yang, *Adv. Energy Mater*. **2018**, *8*, 1702619.
[85] J. Han, H. Zhang, A. Varzi, S. Passerini, *ChemElectroChem*, **2018**, *11*, 3704-3707.
[86] K. Nakamoto, R. Sakamoto, Y. Sawada, M. Ito, S. Okada, *Small Methods*, **2019**, *3*, 1800220.
[87] P. Horcajada, C. Serre, G. Maurin, N. A. Ramsahye, F. Balas, M. Vallet-Regi, M. Sebban, F. Taulelle, G. Férey, *J. Am. Chem. Soc.*, **2008**, *130*, 6774-6780.
[88] G. Férey, F. Millange, M. Morcrette, C. Serre, M.-L. Doublet, J.-M. Grenèche, J. M. Tarascon, *Angew. Chem. Int. Ed.*, **2007**, *46*, 3259-3263.
[89] G. D. Combarieu, M. Morcrette. F. Millange, N. Guillou, J. Cabana, C. P. Gray, I. Margioaki, G. Férey, J. M. Tarascon, *Chem. Mater.*, **2009**, *21*, 1602-1611.

[90] A. Fateeva, P. Horcajada, T. Devic, C. Serre, J. Marrot, J.-M. Grenèche, M. Morcrette, J.-M. Tarascon, G. Maurin, G. Férey, *Eur. J. Inorg. Chem.*, **2010**, *2010*, 3789-3794.

[91] J. Shin, M. Kim, J. Cirera, S. Chen, G. J. Halder, T. A. Yersak, F. Paesani, S. M. Cohen, Y. S. Meng, *J. Mater. Chem. A*, **2015**, *3*, 4738-4744.

[92] T. L. A. Nguyen, T. Devic, P. Mialane, E. Rivière, A. Sonnauer, N. Stock, R. Demir-Cakan, M. Morcrette, C. Livage, J. Marrot, J. M. Tarascon, G. Férey, *Inorg Chem*, **2010**, *49*, 10710-10717.

[93] W. Kaveevivitchai, A. J. Jacobson, *J. Power Sources.*, **2015**, *278*, 265-273.

[94] T. L. A. Nguyen, R. Demir-Cakan, T. Devic, M. Morcrette, T. Ahnfeldt, P. Auban-Senzier, N. Stock, A.-M. Goncalves, Y. Filinchuk, J.-M. Tarascon, G. Férey, *Inorg Chem*, **2010**, 49, 7135-7143.

[95] Z. Zhang, H. Yoshikawa, K. Awaga, *J. Am. Chem. Soc.*, **2014**, *136*, 16112-16115.

[96] M. A. Yanuar, J. Kim, *Carbon*, **2019**, *149*, 483-491.

[97] Q. Zhang, N. N. Liu, C. Z. Sun, L. S. Fan, N. Q. Zhang, K. N. Sun, *ChemElectroChem*, **2019**, *6*, 2189-2194.

[98] P. F. Qi, Y. Z. Han, J. W. Zhou, X. T. Fu, S. W. Li, J. S. Zhao, L. Wang, X. X. Fan, B. Wang, *Chem. Commun.*, **2015**, *51*, 12391-12394.

[99] X. L. Xu, C. Y. Qi, Z. D. Hao, H. Wang, J. T. Jiu, J. B. Liu, H. Yan, K. Suganuma, *Nano-Micro Lett.*, **2017**, *10*: 1.

[100] Y. X. Xie, S. Z. Chen, Z. Y. Lin, W. Yang, H. B. Zou, R. W. Y. Sun, *Electrochem Commun.*, **2019**, *99*, 65-70.

[101] Y. X. Liao, C. Li, X. B. Lou, X. S. Hu, Y. Q. Ning, F. Y. Yuan, B. Chen, M. Shen, B. W. Hu, *Electrochimica Acta*. **2018**, *271*, 608-616.

[102] Y. Z. Han, P. F. Qi, S. W. Li, X. Feng, J. W. Zhou, H. W. Li, S. Y. Su, X. G. Li, B. Wang, *Chem. Commun.*, **2014**, *50*, 8057-8060.

[103] G. H. Zhang, S. C. Hou, H. Zhang, W. Zeng, F. L. Yan, C. C. Li, H. G Duan, *Adv. Mater.*, **2015**, *27*, 2400-2405.

[104] Y. Z. Han, P. F. Qi, X. Feng, S. W. Li, X. T. Fu, H. W. Li, Y. F. Chen, J. W. Zhou, X. G. Li, B. Wang, *ACS appl. Mater. Interfaces.*, **2015**, *7*, 2178-2182.

[105] J. H. Dou, L. Sun, Y. C. Ge, W. B. Li, C. H. Hendon, J. Li, S. Gul, J. Yano, E. A. Stach, M. Dincă, *J. Am. Chem. Soc.*, **2017**, *139*, 13608-13611.

[106] G. Y. Xu, B. Ding, J. Pan, P. Nie, L. F. Shen, X. G. Zhang, *J. Mater. Chem. A*, **2014**, *2*, 12662-12676.

[107] Y. Yang, G. Y. Zheng, Y. Cui, *Chem. Soc. Rev.*, **2013**, *42*, 3018-3032.

[108] G. Y. Xu, J. R. Yuan, X. Y. Tao, B. Ding, H. Dou, X. H. Yan, Y. Xiao, X. G. Zhang, *Nano Res.*, **2015**, *8*, 3066-3074.

[109] H. B. Wu, S. Y. Wei, L. Zhang, R. Xu, H. H. Hng, X. W. Lou, *Chem. Eur. J.*, **2013**, *19*, 10804-10808.

[110] A. Manthiram, Y. Z. Fu, Y. S. Su, *Accounts Chem. Res.*, **2013**, *46*, 1125-1134.

[111] M. L. Li, Y. Wan, J. K. Huang, A. H. Assen, C. E. Hsiung, H. Jiang, Y. Han, M. Eddaoudi, Z.-P. Lai, J. Ming, L. J. Li, *ACS Energy Lett.*, **2017**, *2*, 2362-2367.

[112] X. L. Ji, S. Evers, R. Black, L. F. Nazar, *Nat. Commun.*, **2011**, *2*, 325.

[113] Z. W. Seh, W. Y. Li, J. J. Cha, G. Y. Zheng, Y. Yang, M. T. McDowell, P. C. Hsu, Y. Cui, *Nat. Commun.*, **2013**, *4*, 1331.

[114] D. P. Dubal, K. Jayaramulu, J. Sunil, Š. Kment, P. Gomez-Romero, C. Narayana, R. Zbořil, R. A. Ficher, *Adv. Funct Mater.*, **2019**, *29*, 1900532.

[115] X. Y. Tao, J. G. Wang, C. Liu, H. T. Wang, H. B. Yao, G. Y. Zheng, Z. W. Seh, Q. X. Cai, W. Y. Li, G. M. Zhou, C. X. Zu, Y. Cui, *Nat. Commun.*, **2016**, *7*, 11203.

[116] Q. Q. Wang, J. B. Huang, G. R. Li, Z. Lin, B. H. Liu, Z. P. Li, *J. Power Sources*, **2017**, *339*, 20-26.

[117] Y. S. Su, A. Manthiram, *Nat. Commun.*, **2012**, *3*, 1166.

[118] R. Demir-Cakan, M. Morcrette, F. Nouar, C. Davoisne, T. Devic, D. Gonbeau, R. Dominko, C. Serre, G. Férey, J. M. Tarascon, *J. Am. Chem. Soc.*, **2011**, *133*, 16154-16160.

[119] Y. Y. Mao, G. R. Li, Y. Guo, Z. P. Li, C. D. Liang, X. S. Peng, Z. Lin, *Nat. commun.*, **2017**, *8*, 14628.

[120] J. W. Zhou, R. Li, X. X. Fan, Y. F. Chen, R. D. Han, W. Li, J. Zheng, B. Wang, X. G. Li, *Energy Environ. Sci.*, **2014**, *7*, 2715-2724.

[121] H. Park, D. J. Siegel, *Chem. Mater.*, **2017**, *29*, 4932-4939.

[122] X. F. Liu, X. Q. Guo, R. Wang, Q. C. Liu, Z. J. Li, S. Q. Zang, T. C. W. Mak, *J. Mater. Chem. A*, **2019**, *7*, 2838-2844.

[123] X. J. Hong, T. X. Tan, Y. K. Guo, X. Y. Tang, J. Y. Wang, W. Qin, Y. P. Cai, *Nanoscale*, **2018**, *10*, 2774-2780.

[124] Z. X. Zhao, S. Wang, R. Liang, Z. Li, Z. C. Shi, G. H. Chen, *J. Mater. Chem. A*, **2014**, *2*, 13509-13512.

[125] G. P. Hao, C. Tang, E. Zhang, P. Y. Zhai, J. Yin, W. C. Zhu, Q. Zhang, S. Kaskel, *Adv. Mater.*, **2017**, *29*, 1702829.

[126] H. Zhang, W. Q. Zhao, M. C. Zou, Y. S. Wang, Y. J. Chen, L. Xu, H. S. Wu, A. Y. Cao, *Adv. Funct. Mater*. **2018**, *8*, 1800013.

[127] A. Morozan, F. Jaouen, *Energy Environ. Sci.*, **2012**, *5*, 9269-9290.

[128] M. Hu, J. Reboul, S. Furukawa, N. L. Torad, Q. M. Ji, P. Srinivasu, K. Ariga, S. Kitagawa, Y. Yamauchi, *J. Am. Chem. Soc.*, **2012**, *134*, 2864-2867.

[129] K. Xi, S. Cao, X. Y. Peng, C. Ducati, R. V. Kumar, A. K. Cheetham, *Chem. Commun.*, **2013**, *49*, 2192-2194.

[130] G. Y. Xu, B. Ding, L. F. Shen, P. Nie, J. P. Han, X. G. Zhang, *J. Mater. Chem. A*, **2013**, *1*, 4490-4496.

[131] X. F. Yang, N. Yan, W. Zhou, H. Z. Zhang, X. F. Li, H. M. Zhang, *J. Mater. Chem. A*, **2015**, *3*, 15314-15323.

[132] K. Chen, Z. H. Sun, R. P. Fang, Y. Shi, H. M. Cheng, F. Li, *Adv. Funct. Mater*., **2018**, *28*, 1707592.

[133] Z. Q. Li, L. W. Yin, *ACS Appl. Mater. Interfaces.*, **2015**, *7*, 4029-4038.

[134] A. Abouimrane, D. Dambournet, K. W. Chapman, P. J. Chupas, W. Weng, K. Amine, *J. Am. Chem. Soc.*, **2012**, *134*, 4505-4508.

[135] C. P. Yang, S. Xin, Y. X. Yin, H. Ye, J. Zhang, Y. G. Guo, *Angew. Chem. Int. Ed.*, **2013**, *125*, 8521-8525.

[136] Y. J. Cui, A. Abouimrane, J. Lu, T. Bolin, Y. Ren, W. Weng, C. J. Sun, V. A. Maroni, S. M. Heald, K. Amine, *J. Am. Chem. Soc.*, **2013**, *135*, 8047-8056.

[137] T. Liu, Y. Zhang, J. K. Hou, S. Y. Lu, J. Jiang, M. W. Xu, *RSC Adv.*, **2015**, *5*, 84038-84043.

[138] J. T. Xu, J. M. Ma, Q. H. Fan, S. J. Guo, S.-X. Dou, *Adv. Mater.*, **2017**, *29*, 1606454.

[139] J. Jin, X. C. Tian, N. Srikanth, L. B. Kong, K. Zhou, *J. Mater. Chem. A*, **2017**, *5*, 10110-10126.

[140] T. Liu, M. Jia, Y. Zhang, J. Han, Y. Li, S. J. Bao, D. Y. Liu, J. Jiang, M. W. Xu, *J. Power Sources.*, **2017**, *341*, 53-59.

[141] T. Liu, C. L. Dai, M. Jia, D. Y. Liu, S. J. Bao, J. Jiang, M. W. Xu, C. M. Li, *ACS Appl. Mater. Interfaces.*, **2016**, *8*, 16063-16070.

[142] Z. Q. Li, L. W. Yin, *Nanoscale*, **2015**, *7*, 9597-9606.

[143] J. P. Song, L. Wu, W. D. Dong, C. F. Li, L. H. Chen, X. Dai, C. Li, H. Chen, W. Zou, W. B. Yu, Z. Y. Hu, J. Liu, H. E. Wang, Y. Li, B. L. Su, *Nanoscale*, **2019**, *11*, 6970-6981.

[144] W. D. Dong, H. Chen, F. J. Xia, W. B. Yu, J. P. Song, S. J. Wu, Z. Deng, Z. Y. Hu, T. Hasan, Y. Li, H. G. Wang, L. H. Chen, B. L. Su, *J. Mater. Chem. A*, **2018**, *6*, 22790-22797.

[145] J. J. Xu, Q. C. Liu, Y. Yu, J. Wang, J. M. Yan, X. B. Zhang, *Adv. Mater.*, **2017**, *29*, 1606552.

[146] H. D. Lim, B. Lee, Y. Bae, H. Park, Y. Ko, H. Kim, J. Kim, K. Kang, *Chem. Soc. Rev.*, **2017**, *46*, 2873-2888.

[147] B. Zhou, L. M. Guo, Y. T. Zhang, J. W. Wang, L. P. Ma, W. H. Zhang, Z. W. Fu, Z. Q. Peng, *Adv. Mater.*, **2017**, *29*, 1701568.

[148] Y. G. Zhu, Q. Liu, Y. C. Rong, H. M. Chen, J. Yang, C. K. Jia, L. J. Yu, A. Karton, Y. Ren, X.-X. Xu, S. Adams, Q. Wang, *Nat. Commun.*, **2017**, *8*, 14308.

[149] H. Yadegari, M. N. Banis, A. Lushington, Q. Sun, R. Y. Li, T. K. Sham, X. L. Sun, *Energy Environ. Sci.*, **2017**, *10*, 286-295.

[150] J. Yi, S. H. Guo, P. He, H. S. Zhou, *Energy Environ. Sci.*, **2017**, *10*, 860-884.

[151] N. N. Feng, P. He, H. S. Zhou, *Adv. Energy Mater.*, **2016**, *6*, 1502303.

[152] C. Z. Yang, R. A. Wong, M. Hong, K. Yamanaka, T. Ohta, H. R. Byon, *Nano lett.*, **2016**, *16*, 2969-2974.

[153] D. F. Wu, Z. Y. Guo, X. B. Yin, Q. Q. Pang, B. B. Tu, L. J. Zhang, Y. G. Wang, Q. W. Li, *Adv. Mater.*, **2014**, *26*, 3258-3262.

[154] M. M. O. Thotiyl, S. A. Freunberger, Z. Q. Peng, Y. H. Chen, Z. Liu, P. G. Bruce, *Nat. Mater.*, **2013**, *12*, 1050-1056.

[155] Z. Q. Peng, S. A. Freunberger, Y. H. Chen, P. G. Bruce, *Science*, **2012**, *337*, 563-566.

[156] Q. Li, P. Xu, W. Gao, S. G. Ma, G. Q. Zhang, R. G. Cao, J. Cho, H. L. Wang, G. Wu, *Adv. Mater.*, **2014**, *26*, 1378-1386.

[157] O. Kozachuk, I. Luz, F. X. L. Xamena, H. Noei, M. Kauer, H. B. Albada, E. D. Bloch, B. Marler, Y. M. Wang, M. Muhler, R. A. Fisher, *Angew. Chem. Int. Ed.*, **2013**, *53*, 1-6.

[158] W. Yin, Y. Shen, F. Zou, X. L. Hu, B. Chi, Y. H. Huang, *ACS Appl. Mater. Interfaces.*, **2015**, *7*, 4947-4954.

[159] J. Zhang, L. J. Wang, L. L. Xu, X. M. Ge, X. Zhao, M. Lai, Z. L. Liu, W. Chen, *Nanoscale*, **2015**, *7*, 720-726.

[160] Z. C. Zhang, Y. F. Chen, S. He, J. C. Zhang, X. B. Xu, Y. Yang, F. Nosheen, F. Saleem, W. He, X. Wang, *Angew. Chem. Int. Ed.*, **2014**, *53*, 12517-12521.

[161] Z. Y. Lyu, G. J. H. Lim, R. Guo, Z. K. Kou, T. T. Wang, C. Guan, J. Ding, W. Chen, J. Wang, *Adv. Funct. Mater*, **2019**, *29*, 1806658.

[162] Y. Qiao, Y. B. He, S. C. Wu, K. Z. Jiang, X. Li, S. H. Guo, P. He, H. S. Zhou, ACS Energy Lett., 2018, *3*, 463-468.

[163] M. Shah, M. C. McCarthy, S. Sachdeva, A. K. Lee, H. K. Jeong, *Ind. Eng. Chem. Res.*, **2012**, *51*, 2179-2199.

[164] L. J. Cao, F. C. Lv, Y. Liu, W. X. Wang, Y. F. Huo, X. Z. Fu, R. Sun, Z. G. Lu, *Chem. Commun.*, **2015**, *51*, 4364-4367.

[165] Y. Feng, Y. L. Zhang, G. X. Du, J. B. Zhang, M. Liu, X. H. Qu, *New J. Chem*, **2018**, *42*, 13775-13783.

[166] J. Xu, W. X. Zhang, Y. Chen, H. B. Fan, D. W. Su, G. X. Wang, *J. Mater. Chem. A*, **2018**, *6*, 2797-2807.

[167] B. Hu, X. B. Lou, C. Li, F. S. Geng, C. Zhao, J. Y. Wang, M. Shen, B. W. Hu, *J. Power Sources*, **2019**, *438*, 226954

[168] A. Nichelson, K. Karuppasamy, S. Thanikaikarasan, P. A. Reddy, P. Kollu, S. Karthickprabhu, X. S. Shajan, *Ionics*, **2018**, *24*, 1007-1017.

[169] Z. Y. Wang, W. He, X. D. Zhang, X. L. Yi, J. C. Wang, G. H. Yang, Y. Z. Yue, RSC Adv., 2017, *7*, 21848-21855.

[170] Z. Y. Wang, W. He, X. D. Zhang, Y. Z. Yue, G. H. Yang, X. L. Yi, Y. Y. Wang, J. C. Wang, ChemElectroChem, 2017, *4*, 671-678.

[171] Q. Ni, Y. Bai, Y. Li, L. M. Ling, L. M. Li, G. H. Chen, Z. H. Wang, H. X. Ren, F. Xu, C. Wu, *Small*, **2018**, *14*, 1702864.

10.1002/celc.201900843

WILEY-VCH

REVIEW

The electrochemical performances of the cathodes in batteries are facing a limit. To break this limit, one of the promising ways is to develop the cathode materials by taking advantage of metal organic frameworks (MOFs) owing to tailorable nano-structure. we wrote this review article to describe both opportunities and challenges in developing nanostructured MOF-based cathodes.

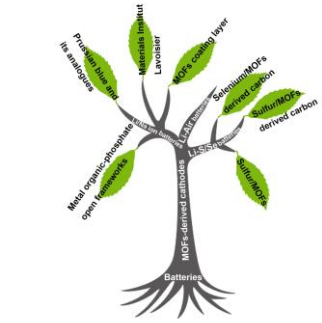

Zhaoyang Wang, Haizheng Tao, Yuanzheng Yue**

Page No. – Page No.

Metal-organic frameworks based cathodes for enhancing electrochemical performances of batteries: a review